Using dissolved H_2O in rhyolitic glasses to estimate palaeo-ice thickness during a subglacial eruption at Bláhnúkur(Torfajökull, Iceland)

Bull Volcanol
DOI 10.1007/s00445-012-0601-5

RESEARCH ARTICLE

Using dissolved H_2O in rhyolitic glasses to estimate palaeo-ice thickness during a subglacial eruption at Bláhnúkur (Torfajökull, Iceland)

Jacqueline Owen · Hugh Tuffen · David W. McGarvie

Received: 18 May 2011 / Accepted: 23 March 2012

Abstract The last decade has seen the refinement of a technique for reconstructing palaeo-ice thicknesses based on using the retained H_2O and CO_2 content in glassy eruptive deposits to infer quenching pressures and therefore ice thicknesses. The method is here applied to Bláhnúkur, a subglacially erupted rhyolitic edifice in Iceland. A decrease in water content from ~0.7 wt.% at the base to ~0.3 wt.% at the top of the edifice suggests that the ice was 400 m thick at the time of the eruption. As Bláhnúkur rises 350 m above the surrounding terrain, this implies that the eruption occurred entirely within ice, which corroborates evidence obtained from earlier lithofacies studies. This paper presents the largest data set (40 samples) so far obtained for the retained volatile contents of deposits from a subglacial eruption. An important consequence is that it enables subtle but significant variations in water content to become evident. In particular, there are anomalous samples which are either water-rich (up to 1 wt.%) or water-poor (~0.2 wt.%), with the former being interpreted as forming intrusively within hyaloclastite and the latter representing batches of magma that were volatile-poor prior to eruption. The large data set also provides further insights into the strengths and weaknesses of using volatiles to infer palaeo-ice thicknesses and highlights many of the uncertainties involved. By using examples from Bláhnúkur, the quantitative use of this technique is evaluated. However, the relative pressure conditions which have shed light on Bláhnúkur's eruption mechanisms and syn-eruptive glacier response show that, despite uncertainties in absolute values, the volatile approach can provide useful insight into the mechanisms of subglacial rhyolitic eruptions, which have never been observed.

Keywords Subglacial · Rhyolite · Degassing · Water solubility · Infra-red spectroscopy · FTIR · Iceland

Editorial responsibility: D.B. Dingwell

Electronic supplementary material The online version of this article (doi:10.1007/s00445-012-0601-5) contains supplementary material, which is available to authorized users.

J. Owen (✉) · H. Tuffen
Lancaster Environment Centre, Lancaster University,
Lancaster LA1 4YQ, UK
e-mail: j.owen2@lancaster.ac.uk

H. Tuffen
e-mail: h.tuffen@lancaster.ac.uk

D. W. McGarvie
Department of Earth and Environmental Sciences,
The Open University,
Milton Keynes MK7 6AA, UK
e-mail: d.mcgarvie@open.ac.uk

Introduction

How volatiles can be used to reconstruct ice thickness

The use of magmatic degassing signatures to reconstruct palaeo-environments was first explored in the 1960s (McBirney 1963; Moore 1965; Jones 1969; Moore 1970) based on the observation that vesicle percentage, and vesicle diameter increased with decreasing depth of marine pillow lavas (Moore 1965; Jones 1969). However, the first attempt to quantitatively model the relationship between vesicle volume and depth came much later (Macpherson 1984). In the meantime, considerable work had been done determining the solubility of water (H_2O) and carbon dioxide (CO_2), the two main components of the vapour phase in silicic melts; see Mysen (1977) for a review. This led Newman et al. (1988) to produce the first volatile saturation model for rhyolites; Dixon and Stolper (1995) then produced the

Published online: 24 April 2012

equivalent for basalts and Dixon (1997) for alkalic basalts. Papers such as these provided the foundation for compositionally sensitive volatile saturation models such as VolatileCalc (Newman and Lowenstern 2002) and the models of Moore et al. (1998) and Papale et al. (2006). These use volatile solubility relationships to enable the calculation of quenching pressures based on the amount of undegassed H_2O and CO_2.

In a simple subglacial eruptive environment (i.e. assuming that cavity pressure at the eruption site is equal to glaciostatic pressure and that the loading medium is a thick ice sheet of uniform density), the pressure that the ice exerts on material erupting and quenching at the base of the ice sheet will be dependent only on the thickness of the overlying ice (Tuffen et al. 2010). Thus, the dissolved H_2O and CO_2 content of the eruptives, with the application of a suitable solubility model, yields a palaeo-ice thickness. This has been demonstrated in several studies, e.g. Dixon et al. (2002), Schopka et al. (2006), Höskuldsson et al. (2006), Tuffen et al. (2008), Edwards et al. (2009), Stevenson et al. (2009) and Tuffen and Castro (2009).

Before the application of magma degassing analyses to reconstruct palaeo-ice thicknesses, reconstruction tools relied on lithofacies interpretation, either using the subglacial to subaerial transition of eruptions that emerged through the ice-sheet to produce substantial tuyas (table mountains) (Mathews 1947; Jones 1966; Tuffen et al. 2002a; Edwards et al. 2011), or the recognition of entirely subglacial edifices whose height thus provides a minimum ice thickness (Tuffen et al. 2001; McGarvie et al. 2007; Tuffen et al. 2010). Thus, the use of magma degassing signatures increases the potential for reconstructing palaeo-ice thicknesses from erupted deposits.

Palaeo-ice thickness reconstructions are valuable for understanding volcano–ice interactions (Smellie and Skilling 1994; Smellie 2000; Guðmundsson 2005; Tuffen et al. 2007; Stevenson et al. 2009) and characterising past environmental change (Smellie 2000; Smellie 2008; McGarvie 2009). If edifices can be radiometrically dated subglacially, erupted deposits provide useful snapshots of ice sheet thickness at a given time (McGarvie et al. 2006; Smellie et al. 2008; McGarvie 2009; Tuffen et al. 2010; Edwards et al. 2011). As a link between deglaciation and increased volcanism is becoming increasingly recognised (Sigvaldason et al. 1992; Jull and McKenzie 1996; Maclennan et al. 2002; Tuffen 2011), reconstruction of palaeo-ice thicknesses on volcanoes yields key information about this relationship, within the context of a potential acceleration in twenty-first-century volcanism as glaciers thin in a warming world (Tuffen 2010).

Dissolved volatile contents may additionally provide information on syn-eruptive subglacial hydrology (Höskuldsson et al. 2006; Schopka et al. 2006) and past loading conditions imposed by overburden that has since been eroded away (Stevenson et al. 2009; Tuffen and Castro 2009). These inferences have been made by comparing expected ice thicknesses based on field interpretation with those estimated from dissolved volatile concentrations (Tuffen and Castro 2009), or by examining the relationship between dissolved volatile content and elevation (Schopka et al. 2006; McGarvie et al. 2007).

A decreasing trend of water content with elevation is expected if quenching pressures reflect the weight of an overlying flat-topped ice sheet, as edifice construction lessens the thickness of overlying ice (Dixon et al. 2002; Schopka et al. 2006; Tuffen et al. 2010). This can be modelled using a solubility model such as VolatileCalc (Newman and Lowenstern 2002) and a solubility pressure curve (SPC) constructed, but this has only been applied to one eruption (Schopka et al. 2006). Use of SPCs improves the robustness of palaeo-ice reconstructions, as it allows modelling of expected water contents over a range of elevations and pressures, allowing comparison with large datasets, rather than isolated individual samples.

In this paper, we present the most detailed application so far undertaken of the magma degassing technique to a subglacial eruption. This allows (1) determination of palaeo-ice thickness during the subglacial rhyolite eruption of Bláhnúkur in southern Iceland; (2) clearer insights into complicating factors that have not been fully recognised in past studies; (3) further evaluation of the advantages and disadvantages of using H_2O and CO_2 contents to reconstruct palaeo-ice thicknesses and (4) improved understanding of the mechanisms of effusive rhyolitic eruptions under ice.

Bláhnúkur and its geological setting

Bláhnúkur occurs within the Torfajökull central volcano complex, which is the largest silicic centre in Iceland (Sæmundsson 1972; McGarvie 1985; Gunnarsson et al. 1998). Torfajökull is located in southern Iceland where the Eastern Rift Zone (ERZ) meets the Southern Flank Zone (SFZ) (Fig. 1a). Sæmundsson (1972) estimates that the complex has been active since ~1 Ma. More than 250 km^3 of rhyolite has been erupted at the complex in numerous, mostly subglacial eruptions (McGarvie 1985). Holocene rhyolite eruptions at Torfajökull have been triggered by laterally propagating tholeiitic dykes from the ERZ intersecting rhyolitic magma chambers beneath Torfajökull (Blake 1984; Larsen 1984; McGarvie 1984; Mørk 1984; McGarvie et al. 1990). These dykes propagated from the Veiðivötn system and have originated from Bárðarbunga central volcano (Fig. 1a) (Larsen 1984; McGarvie 1985). There is similar evidence of magma mixing/mingling within some (but not all) Weichselian subglacial rhyolite eruptions (McGarvie et al. 2006). The most recent eruption occurred in 1477 (McGarvie et al. 1990).

Bláhnúkur is located in the NE part of Torfajökull (Fig. 1b) and was formed in a small-volume (<0.1 km^3) subglacial rhyolitic eruption (Furnes et al. 1980; Tuffen et

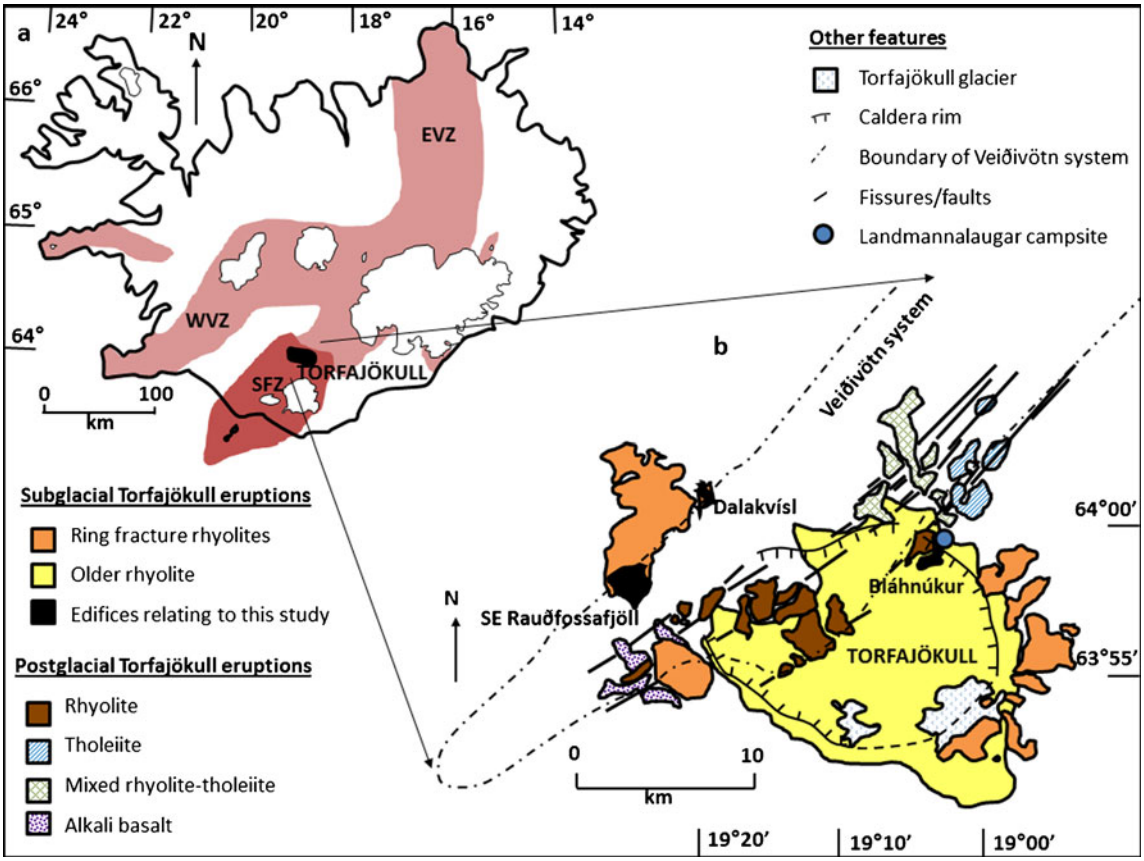

Fig. 1 **a** Simplified geological map of Iceland, based on Gunnarsson et al. (1998) and Larsen (1984) **b** Simplified geological map of Torfajökull, based on Gunnarsson et al. (1998); McGarvie (1984); McGarvie et al. (2006) and Blake (1984)

al. 2001; Tuffen et al. 2002b). The edifice is pyramidal in form and has a summit at 945 masl that rises 350 m above a rhyolitic plateau at ~600 masl. The eruptive products form a thin (c.50 m) blanket over the upper flanks of an old rhyolitic hill (Fig. 2) and are dominated by quench hyaloclastite and lava lobe lithofacies considered typical of an effusive, entirely subglacial eruption of rhyolite (Tuffen et al. 2001). The constituent rhyolite is micro-porphyritic (predominantly feldspars with some pyroxenes), subalkaline, and contains 1–8 vol.% of discrete inclusions, mostly <7 mm across that consist of mafic rock (McGarvie 1985). Lava lobes protrude out of the hyaloclastite like 'warts' (Sæmundsson 1972) (Fig. 2a), are ~5–10 m across and thought to have formed either within subglacial cavities at the ice–edifice interface (Tuffen 2001, 2002b), or intrusively within hyaloclastite (Stevenson et al. 2011). The edifice is Pleistocene in age (McGarvie et al. 2006) and probably erupted within the Weichselian glacial period based on a lesser degree of alteration than the older rhyolitic formations (Fig. 2a).

Constraints on inferred ice thickness at Bláhnúkur

As diagnostic subaerial features are lacking from the preserved lithofacies at Bláhnúkur, the eruption is thought to have remained entirely subglacial (Tuffen et al. 2001, 2002b). This requires ice ≥350 m thick. However, the depth of ice cauldrons observed during the 1996 Gjálp eruption was >50 m (Guðmundsson et al. 2004); so, if we assume a broadly similar heat flux and ice deformation response occurred, this suggests that ≥400 m of ice was present during the Bláhnúkur eruption (Tuffen et al. 2001, 2007; McGarvie 2009). This is similar to ice thickness estimates derived from inferred subglacial–subaerial transitions at nearby rhyolitic tuyas (Tuffen et al. 2002a; McGarvie et al. 2006), which have been dated to 67±9 and 71.5±7.4 ka (McGarvie et al. 2006).

Methods

Sampling methods

A total of 40 samples were collected at a range of elevations from lava lobe margins, dykes, and other lava bodies (Table 1). All collected samples were glassy throughout, and hydrated (perlitised) samples were avoided wherever possible, as were localities that showed evidence of post-quenching movement. One sample contained a mafic

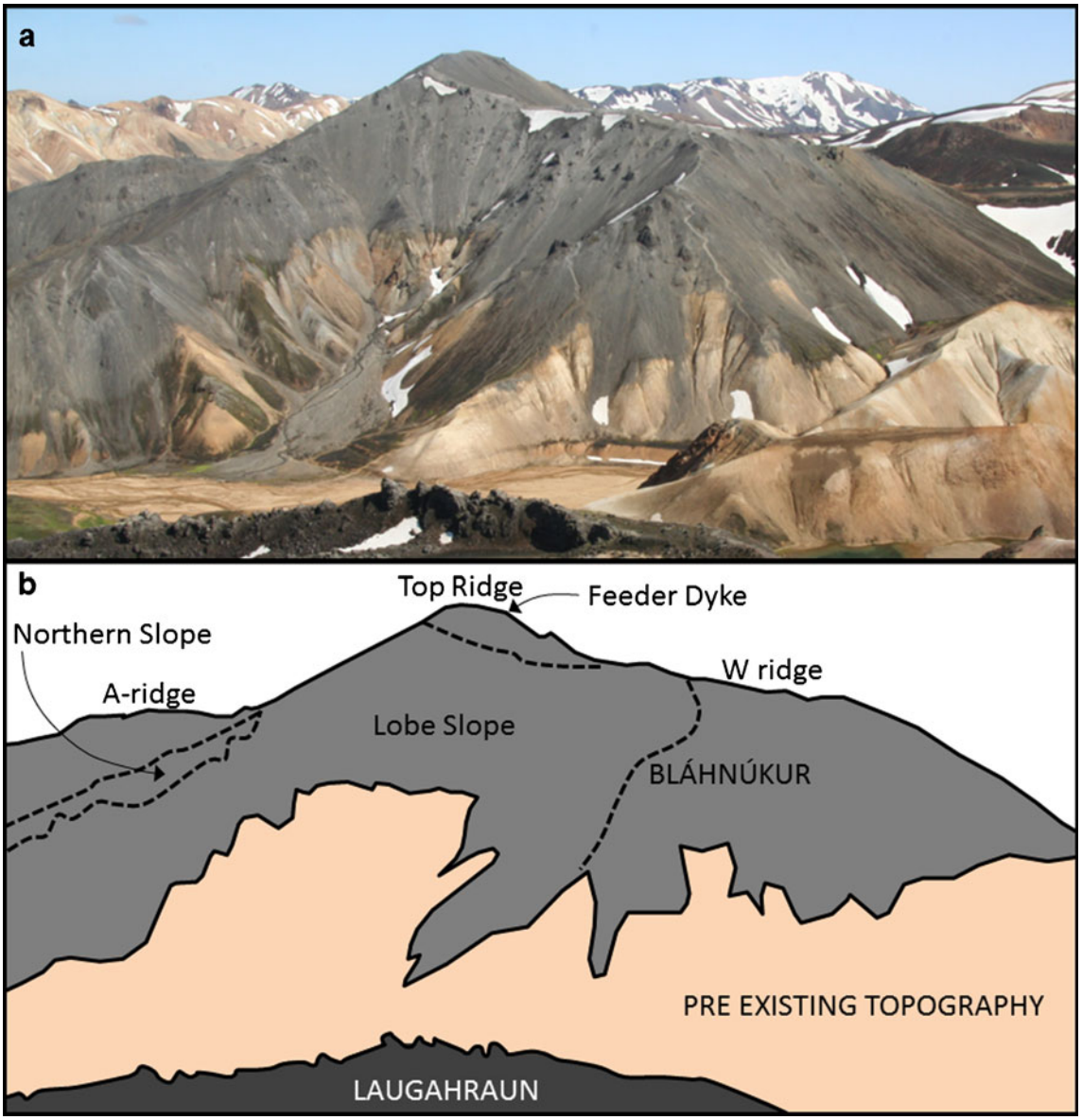

Fig. 2 **a** Bláhnúkur photographed eastward from Brennisteinsalda towards the 'Lobe Slope' where lava lobes protrude from hyaloclastite. Orange material at the edifice base is older rhyolite overlain by grey Bláhnúkur subglacial rhyolite. **b** Schematic representation of Fig. 2a, with different colours depicting Bláhnúkur, the pre-existing topography and the 1477 AD lava flow Laugahraun. *Dashed lines* mark the prominent ridges of Bláhnúkur and some of the sampling locations are labelled

inclusion several centimeters across, with a discrete but crenulated contact with the obsidian. This inclusion was analysed for geochemistry.

Geochemistry: XRF

Major and trace element compositions of six samples were determined at the X-ray fluorescence (XRF) facility at the University of Edinburgh, UK, using a Panalytical PW2404 wavelength-dispersive sequential X-ray spectrometer. The six samples were chosen to cover a wide range of lithofacies, water contents and elevations in order to obtain the most representative data-set possible (Table 1). Accuracy and precision were established by repeatedly analysing standards of known composition (Supplementary Table 1).

Dissolved H_2O and CO_2 content: FTIR

Fourier transform infrared (FTIR) spectroscopy was used to determine the concentration of H_2O and CO_2 species in the glass. Samples were cut and doubly polished to create wafers ~100–300 μm thick and thicknesses measured to ±3 μm (according to the manufacturer's product description) with a Mitutoyo digital displacement gauge. FTIR

Table 1 A brief summary of the samples collected, the sampling localities and the analytical work done on each

Sampling location	Sample name	GPS coordinates	Elevation (m)	Reference facies unit[a]	Sample description[b]	Locality description	XRF	FTIR	Ves[d]
A-Ridge	J1	N 63 59 03.9, W 019 03 42.7	681	A	ob	Lava lobe	/	Yes	Yes
	B5	N 63 59 00.1, W 019 03 43.2	703	A	ob	Lava lobe	/	Yes	Yes
	J2b	N 63 58 58.7, W 019 03 43.6	710	A	ob	Lava lobe	Yes	Yes (*x*2)	Yes
	J2f	N 63 58 58.7, W 019 03 43.6	710	A	ob	Lava lobe	/	Yes	Yes
	B6	N 63 58 53.1, W 019 03 47.1	774	A	ob	Lava lobe	/	Yes	Yes
	B7	N 63 58 50.4, W 019 03 44.7	801	A	ob	Lava lobe	/	Yes	Yes
	B8	N 63 58 43.5, W 019 03 47.6	817	A	ob	Lava lobe	/	Yes	Yes
	J8	N 63 58 49.6, W 019 03 46.7	819	A	ob	Lava lobe	/	Yes	Yes
	J9	N 63 58 46.3, W 019 03 46.9	823	A	ob	Lava lobe	/	Yes	Yes
	J10	N 63 58 39.5, W 019 03 55.4	862	cjl	ob	Dyke	/	Yes	Yes
Grænagil	B18	N 63 59 10.0, W 019 03 40.1	614	B	ob	Lava lobe	/	Yes	Yes
	J6	N 63 59 08.8, W 019 03 40.2	612	B	ob	Lava lobe	/	Yes	Yes
	G3a	N 63 59 05.4, W 019 03 45.8	614	B	ob	Lava lobe	/	Yes	Yes
	G3end	N 63 59 05.4, W 019 03 45.8	614	B	ob	Lava lobe	/	Yes	Yes
	J3	N 63 59 03.8, W 019 03 50.6	620	B	ob	Lava lobe	Yes	Yes	Yes
Northern slope	J7	N 63 58 51.6, W 019 03 56.1	730	A	ob	Lava lobe	/	Yes	Yes
Feeder dyke	J11	N 63 58 35.3, W 019 04 08.1	937	cjl	ob	Dyke	Yes	Yes	Yes
	J13	N 63 58 33.4, W 019 04 08.2	920	cjl	ob	Dyke	/	Yes	Yes
	J14	N 63 58 31.9, W 019 04 07.5	900	cjl	ob	Dyke	/	Yes	Yes
Top ridge	B1	N 63 58 36.1, W 019 04 07.3	934	B	ob	Dyke	/	Yes	Yes
	B11	N 63 58 38.1, W 019 04 12.0	935	A	ob	Lava lobe	/	Yes	Yes
W Ridge	J4	N 63 58 28.7, W 019 04 38.1	860	B	ob	Lava lobe	/	Yes	Yes
Brandsgil	B2	N 63 58 49.5, W019 03 21.5	671	cjl	ob	Sill /flow[c]	Yes	Yes	Yes
	B3	N 63 58 49.0, W019 03 24.8	681	cjl	ob	Sill /flow[c]	/	Yes	Yes
	B4	N 63 58 49.0, W019 03 24.8	696	cjl	ob	Sill /flow[c]	/	Yes	Yes
	J16(b)	N 63 58 49.5, W 019 03 21.1	670	cjl	inc	Sill /flow[c]	Yes	/	/
Lobe slope	J5	N 63 58 37.6, W 019 04 21.5	880	A	ob	Lava lobe	/	Yes	Yes
	L6c	N 63 58 39.4, W 019 04 44.6	793	B	vp	Lava lobe	/	Yes	Yes
	L7c	N 63 58 37.2, W 019 04 36.5	816	A	ob	Lava lobe	/	Yes	Yes
	L8d	N 63 58 36.9, W 019 04 26.5	860	A	ob	Lava lobe	Yes	Yes	Yes
	L8bott	N 63 58 36.9, W 019 04 26.5	860	A	ob	Lava lobe	/	Yes	Yes
	L9w	N 63 58 38.0, W 019 04 30.2	830	A	ob	Lava lobe	/	Yes	Yes
	L9y	N 63 58 38.0, W 019 04 30.2	830	A	ob	Lava lobe	/	Yes	Yes
	L9z	N 63 58 38.0, W 019 04 30.2	830	A	ob	Lava lobe	/	Yes	Yes
	L11c	N 63 58 36.1, W 019 04 29.4	880	A	ob	Lava lobe	/	Yes	Yes
	B12	N 63 58 43.9, W 019 04 20.1	896	A	ob	Lava lobe	/	Yes	Yes
	B13	N 63 58 36.4, W 019 04 21.1	880	A	ob	Lava lobe	/	Yes	Yes
	B14	N 63 58 33.6, W 019 04 25.2	880	A	ob	Lava lobe	/	Yes	Yes
	B15	N 63 58 36.9, W 019 04 44.1	819	B	vp	Lava lobe	/	Yes	Yes
	B16a	N 63 58 39.9, W 019 04 44.9	770	B	vp	Lava lobe	/	Yes	Yes

A lava lobe-breccia A, *B* breccia B, *cjl* columnar jointed lava

[a] The unit to which the sample belongs according to the geological map of Tuffen et al. (2001), where a full description and interpretation of each lithofacies can be found

[b] Sample description where ob=a sample which is pristine obsidian glass throughout; vp=variably perlitised glass, inc=a large mafic inclusion within obsidian

[c] Samples from a lava body where it was unclear in the field whether it formed intrusively or extrusively, i.e. whether it is a sill or a lava flow, respectively

[d] Whether or not vesicularity measurements were undertaken

analysis was carried out using a Thermo Nicolet FTIR at the Open University, UK, with a Continuum Analytical microscope, KBr beamsplitter, MCT-A detector, and 100 μm square aperture. For each data point, 256 scans were collected over 650–5,000 cm^{-1} at 4 cm^{-1} resolution. A minimum of five data points were taken from each sample. To minimize atmospheric contamination, samples were analysed inside a N_2 purged tank, and a background was collected for every sample. Spectra were processed by applying a 15-point linear baseline correction.

Total water (H_2O_t) and molecular water (H_2O_m) contents were measured using the 3,550 and 1,630 cm^{-1} peaks, respectively. Hydroxyl content (OH) is detectable with a 4,520 cm^{-1} peak, but only in samples that have water contents >1 wt.% (Okumura et al. 2003). In rhyolites, the concentration of carbonate groups is negligible; molecular CO_2 is the dominant carbon species, thus total CO_2 can be represented by the molecular CO_2 peak at 2,350 cm^{-1} (Behrens et al. 2004).

Peak heights were converted into H_2O and CO_2 concentrations (C_i) using the Beer-Lambert Law (Stolper 1982b; Leschik et al. 2004), according to the formula

$$C_i = \frac{M_i Abs}{d\rho\varepsilon} \quad (1)$$

where i refers to either H_2O or CO_2, M is the molecular weight of substance i (18.02 $g mol^{-1}$ for H_2O and 44.01 g mol^{-1} for CO_2), Abs is absorbance (measured peak height), d is sample thickness (in centimeters), ρ is rock density (in grams per liter) and ε is the absorption coefficient (in liters per mole per centimeter) that corresponds to the peak height measured. A rock density of 2,470 $g l^{-1}$ was used (see below) and absorption coefficients of 80 (Leschik et al. 2004), 55 (Newman et al. 1986), 1.42 (Okumura and Nakashima 2005) and 1,214 $l mol^{-1}$ cm^{-1} (Behrens et al. 2004) for the 3,550; 1,630; 4,520 and 2,350 cm^{-1} peaks, respectively.

Sample densities were measured using the Archimedes Principle. Using this method, the mean density of non-vesicular samples was 2.47±0.03 $g cm^{-3}$. Three measurements were taken per sample. The precision of the technique was tested using substances of known density, and results were reproducible within 3 %.

Estimated cumulative errors for FTIR measurements are commonly quoted as ±10 % for H_2O_t (Dixon and Clague 2001; Dixon et al. 2002; Nichols and Wysoczanski 2007) and ±20 % for H_2O_m (Dixon and Clague 2001; Dixon et al. 2002).

Estimating vesicularity: bead technique

We used a modified version of the bead displacement technique (Stevenson 2005) to estimate sample vesicularity, using ~1 mm glass beads. Unlike water, beads do not penetrate into smaller vesicles, giving a better indication of volume. Measured densities were adjusted to account for bead packing, using a packing coefficient determined by comparing the bead measured densities of non-vesicular samples with densities determined through the Archimedes Principle. By assuming that all Bláhnúkur obsidian is of approximately the same density (minor adjustments were made for samples bearing mafic inclusions), we estimated sample vesicularity, by comparing the densities of the vesicular samples with those that are non-vesicular.

Sample textures were examined under thin section, and in particular, we sought evidence for bubble collapse and annealing (Westrich and Eichelberger 1994; Tuffen and Castro 2009) and therefore the former presence of vesicles. Volatile saturation is essential if retained magmatic volatiles are to faithfully record quenching pressures (Höskuldsson et al. 2006; Tuffen et al. 2010). The diagnostic sign that volatile saturation has been reached is the presence of vesicles.

Determining the palaeo-ice thickness

We have adopted the method of Schopka et al. (2006), which is to plot H_2O against elevation for a multitude of samples and compare the whole data set to SPCs, determined using solubility models, which represent various loading conditions. We used the solubility model VolatileCalc (Newman and Lowenstern 2002); see section "Which solubility model to use?" for justification. Note that this method is most appropriate where the ice is thick enough for the glacier surface to be independent of sub-surface topography and therefore be approximated as being roughly flat. This is thought to be the case with most ice caps/sheets, away from margins and thus can be applied to the Pleistocene eruption of Bláhnúkur. Development of a syn-eruptive ice cauldron should manifest itself with near vent samples having anomalously low water contents compared with lower elevation samples for a given SPC.

Results

Geochemistry: XRF

XRF data reveal that all glassy samples tested are rhyolitic in composition (Table 2), as previously described (Furnes et al. 1980; Tuffen et al. 2001; McGarvie 2009). However, we also tested one of the discrete, apparently mafic inclusions thought to represent tholeiitic contamination from the Veiðivötn dyke swarm (Larsen 1984; Mørk 1984) and found it to be intermediate in composition (62 wt.% SiO_2), rather than basaltic as previously thought (McGarvie 1985; MacDonald et al. 1990; McGarvie et al. 1990; Tuffen et al.

Table 2 XRF major and trace element chemistry for five samples of obsidian (J2b, J3, J11, L8d and B2) and one "mafic" inclusion (J16(b))

	J2b	J3	J11	L8d	B2	J16(b)
SiO_2	70.68	70.15	69.90	70.51	69.19	61.89
TiO_2	0.283	0.278	0.276	0.280	0.310	0.647
Al_2O_3	14.17	14.11	14.03	14.23	14.01	14.00
Fe_2O_3	3.33	3.30	3.29	3.31	3.54	6.20
MnO	0.086	0.084	0.084	0.082	0.085	0.125
MgO	0.28	0.27	0.27	0.28	0.51	3.19
CaO	0.91	0.90	0.88	0.90	1.24	5.44
Na_2O	5.636	5.613	5.560	5.643	5.417	4.110
K_2O	4.375	4.347	4.334	4.379	4.203	2.764
P_2O_5	0.034	0.033	0.035	0.035	0.035	0.062
LOI	0.49	1.19	0.58	0.28	1.05	1.23
Total	100.28	100.28	99.24	99.94	99.59	99.65
Ba	452.9	450.2	454.6	445.9	434.4	299.4
Sc	0.6	n.d.	n.d.	n.d.	2.1	20.4
V	0.9	0.9	n.d.	n.d.	10.0	113.6
Cr	n.d.	n.d.	n.d.	n.d.	n.d.	n.d.
Cu	7.3	7.5	7.6	8.1	10.9	54.8
Nb	140.5	139.4	140.7	139.1	135.8	89.1
Ni	n.d.	n.d.	n.d.	n.d.	n.d.	n.d.
Pb	8.9	8.8	9.2	9.0	8.6	5.4
Rb	102.9	102.3	103.2	102.2	99.1	63.8
Sr	59.0	58.3	58.6	58.5	59.4	85.7
Th	16.7	16.2	16.7	16.6	16.0	10.4
U	5.0	5.0	5.0	4.9	4.8	3.2
Y	92.0	91.1	92.3	91.1	89.7	66.9
Zn	123.5	124.1	123.0	125.3	123.0	108.8
Zr	875	870.4	893.7	872.1	867.7	573.6
La	107.5	107.4	105.5	106.2	103.7	70.2
Ce	214.6	212.4	211.6	208.8	205.6	143.5
Nd	88.1	87.1	88.2	86.1	85.3	61.3

LOI loss on ignition, *n.d.* none detected

Major elements are in wt.% and trace elements are in ppm

2001). This may suggest a small degree of magma mingling or hybridisation, but more study is needed to reveal the details.

There is little variation between the major element geochemistry of the Bláhnúkur obsidian samples (Fig. 3), supporting the model of a monogenetic eruption. All samples plot on a linear trend that has the "mafic" inclusion as an endmember (Fig. 3). We attribute the slight difference between sample B2, from Brandsgil and the other samples to a greater concentration of inclusions and possible hybridisation (McGarvie (1985), which can explain its lower total alkali and silica contents (Table 2, Fig. 3). Brandsgil samples were notably inclusion-rich.

Trace element data shows little variation amongst the Bláhnúkur rhyolite samples (Table 2, Fig. 4), further supporting the monogenetic eruption model (McGarvie et al. 2007). This is even more apparent when the data is compared with other rhyolitic edifices within Torfajökull, which have very similar major element chemistry (Owen, unpublished data 2010) but significantly different trace element chemistry (Fig. 4).

Dissolved H_2O and CO_2: FTIR

FTIR measurements reveal that the total dissolved water concentration varies between 0.2 and 1 wt.% (see Table 3 for mean values and Supplementary Table 2 for raw values). No discernible 2350 cm^{-1} peaks were detected, indicating CO_2 concentrations below the detection limit of 30 ppm in all samples, and the OH peak (4,520 cm^{-1}) was too weak to measure accurately, as expected for H_2O_t<1 wt.% (Okumura et al. 2003). Variable H_2O_m peaks at 1,630 cm^{-1} may reflect localised post-quenching hydration.

Since meteoric water is added as H_2O_m at low temperatures, hydrated samples have anomalously high H_2O_m/H_2O_t ratios (Yokoyama et al. 2008; Denton et al. 2009). Two samples (L9z and J4) show particularly high ratios of H_2O_m (Table 3) and are suspected to be hydrated. These are labelled separately from all other samples in Fig. 5, where they display a distinctively higher and linear H_2O_m–H_2O_t trend.

Overall, the H_2O_m–H_2O_t trend for non-hydrated samples is similar to published speciation trends (Stolper 1982b; Stolper 1982a; Jakobsson 1997; Ihinger et al. 1999; Zhang 1999; Ohlhorst et al. 2001; Mandeville et al. 2002), but the H_2O_t at which H_2O_m becomes the dominant species is different. This is probably due to the high sensitivity of the speciation ratios to the choice of absorption coefficient and may explain why many samples have higher magmatic H_2O_m/H_2O_t ratios (Table 3) than published values. There are additional complicating factors as speciation is also dependent on composition, magma temperature and cooling rate as well as the absorption coefficients used (Stolper 1982b, a; Silver and Stolper 1989; Silver et al. 1990; Zhang 1999); see section "Which absorption coefficient to use?").

Vesicularity

Vesicularity data and vesicle texture information are provided in Table 4. Vesicles indicate degassing from a volatile-saturated magma, a necessary requirement for reconstructing palaeo-ice thicknesses (Höskuldsson et al. 2006; Tuffen et al. 2010).

Although 11 of the 40 samples are vesicle-free (Table 4), bubbles commonly collapse and heal (Westrich and Eichelberger 1994; Tuffen and Castro 2009), so lack of vesicles does not preclude earlier vesiculation. In thin section, many samples show partly collapsed (i.e. flattened) bubbles, as well as thin and linear wisps that we term "bubble ghosts" and consider to be remnants of

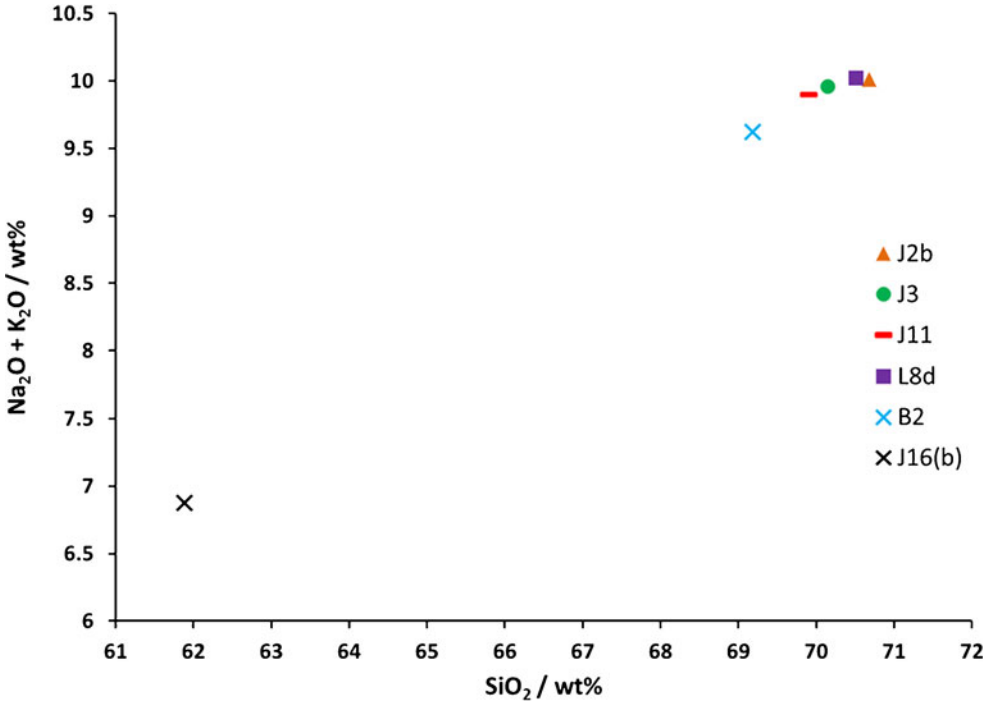

Fig. 3 Major element XRF data for Bláhnúkur. J2b, J3, J11, L8d and B2 are samples of obsidian. J16(b) is a "mafic" inclusion

earlier vesicles (Fig. 6). Some samples such as J11 lack open vesicles, but abundant bubble ghosts indicate earlier vesiculation; these are considered to meet the condition of volatile saturation.

Creating solubility pressure curves

We have constructed SPCs using the VolatileCalc solubility-pressure model (Newman and Lowenstern 2002). Magma composition, CO_2 content and temperature affect water pressure-solubility relationships; their effects are discussed later. XRF data shows that our samples are all rhyolites of uniform composition (Table 2). No CO_2 was detected in our samples, therefore, unless otherwise stated, we assume that the CO_2 content is 0 ppm (although it could be up to 30 ppm as this is the detection limit of the FTIR). The eruption temperature of the Bláhnúkur rhyolite is not known; however, Fe-Ti oxide geothermometry gives eruption temperatures of 750–

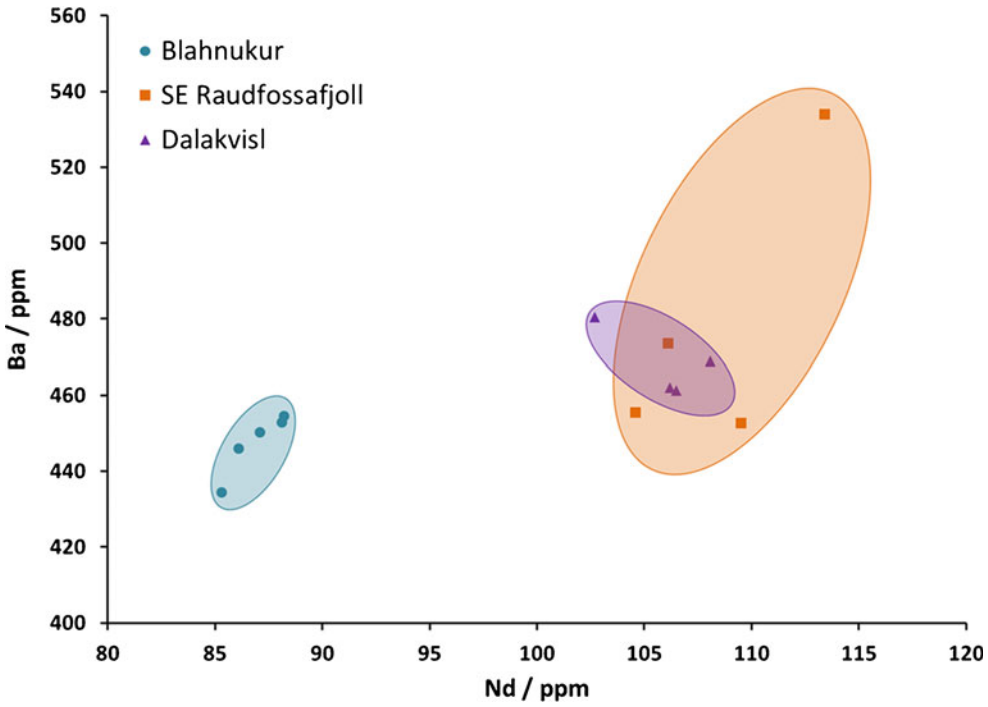

Fig. 4 Trace element data acquired from XRF analysis for Bláhnúkur, SE Rauðfossafjöll and Dalakvísl (shown in Fig. 1b). The latter two are ring fracture rhyolites thought to derive from the same eruptive event (McGarvie et al. 2006). The separation of the Bláhnúkur data from these areas coupled with the strong clustering of the Bláhnúkur data supports the view that Bláhnúkur erupted from a single magma batch

Table 3 FTIR data (H_2O_t and H_2O_m) averaged according to the number of successful measurements per sample

Sample name	Sample thickness (μm)[a]	FTIR points per sample[b]	3550 peak height[c]	1630 peak height[c]	Mean H_2O_t (wt%)[d]	Mean H_2O_m (wt%) [d]	St. dev. H_2O_t (wt%)[e]	St. dev. H_2O_m (wt%)[e]
J1	177	6	0.429	0.168	0.22	0.13	0.01	0.01
B5	278	4	0.870	0.265	0.29	0.13	0.05	0.04
J2b(1)	175/194	19	0.572	0.144	0.29	0.10	0.01	0.01
J2b(2)	255	5	0.954	0.177	0.34	0.09	0.01	0.00
J2f	310	7	0.641	0.180	0.19	0.08	0.01	0.00
B6	96	5	0.444	0.087	0.42	0.12	0.08	0.02
B7	350	5	1.136	0.241	0.30	0.09	0.02	0.01
B8	121	5	0.433	0.241	0.33	0.17	0.02	0.02
J8	187	5	0.756	0.172	0.37	0.12	0.02	0.01
J9	95	6	0.494	0.089	0.47	0.12	0.01	0.00
J10	168	6	0.745	0.206	0.40	0.16	0.01	0.01
B18	187	5	1.095	0.333	0.53	0.24	0.02	0.01
J6	170	5	1.205	0.321	0.65	0.25	0.04	0.02
G3a	162	7	1.280	0.372	0.72	0.30	0.06	0.03
G3end	181	5	1.346	0.438	0.68	0.32	0.08	0.03
J3	177	5	1.162	0.258	0.60	0.19	0.01	0.00
J7	216	5	1.272	0.321	0.54	0.14	0.04	0.01
J11	119	9	0.350	0.110	0.27	0.12	0.01	0.01
J13	185	5	0.638	0.230	0.31	0.16	0.02	0.01
J14	118	5	0.520	0.200	0.40	0.22	0.01	0.00
B1	147	5	0.470	0.160	0.29	0.14	0.02	0.01
B11	176	5	0.533	0.187	0.28	0.14	0.01	0.01
J4	161	5	1.343	0.703	0.76	0.58	0.09	0.08
B2	89	5	0.794	0.256	0.81	0.38	0.04	0.04
B3	69	5	0.649	0.155	0.86	0.30	0.04	0.01
B4	119	5	1.029	0.416	0.79	0.33	0.14	0.12
J5	214	6	1.037	0.307	0.44	0.19	0.03	0.00
L6c	131	5	1.088	0.285	0.76	0.29	0.01	0.01
L7c	124	5	0.960	0.204	0.71	0.22	0.03	0.01
L8d	162	5	1.029	0.250	0.58	0.20	0.02	0.01
L8bott	129/169/163	15	1.109	0.279	0.66	0.24	0.12	0.08
L9w	118	6	1.049	0.275	0.81	0.31	0.06	0.01
L9y	180	5	1.319	0.390	0.67	0.29	0.02	0.03
L9z	120	6	0.435	0.236	0.33	0.26	0.11	0.11
L11c	129	5	0.910	0.200	0.64	0.21	0.01	0.01
B12	108	5	0.822	0.210	0.69	0.26	0.09	0.02
B13	179	5	1.168	0.280	0.59	0.21	0.02	0.00
B14	240	5	1.320	0.274	0.50	0.15	0.01	0.00
B15	110	5	0.656	0.143	0.54	0.17	0.03	0.01
B16a	178	5	1.376	0.350	0.70	0.26	0.02	0.00

In all samples, CO_2 (2,350 cm^{-1} peak) and OH (4,520 cm^{-1} peak) were below detection limit

[a] Single measurement of sample thickness at location within tens of micrometres of FTIR analysis. With the exception of J2b and L8bott where multiple locations on the wafer were measured

[b] Number of FTIR measurements per sample

[c] Mean absorbance levels from the 3,550 cm^{-1} (total water) and 1,630 cm^{-1} (molecular water) peaks

[d] Mean total (H_2O_t) water content and molecular (H_2O_m) water contents calculated using the Beer-Lambert law, assuming a density of 4,272.5 gcm^{-3} and absorption coefficients of 80 and 55 $lmol^{-1}$ cm^{-1}, respectively

[e] Standard deviation on total (H_2O_t) and molecular (H_2O_m) water contents

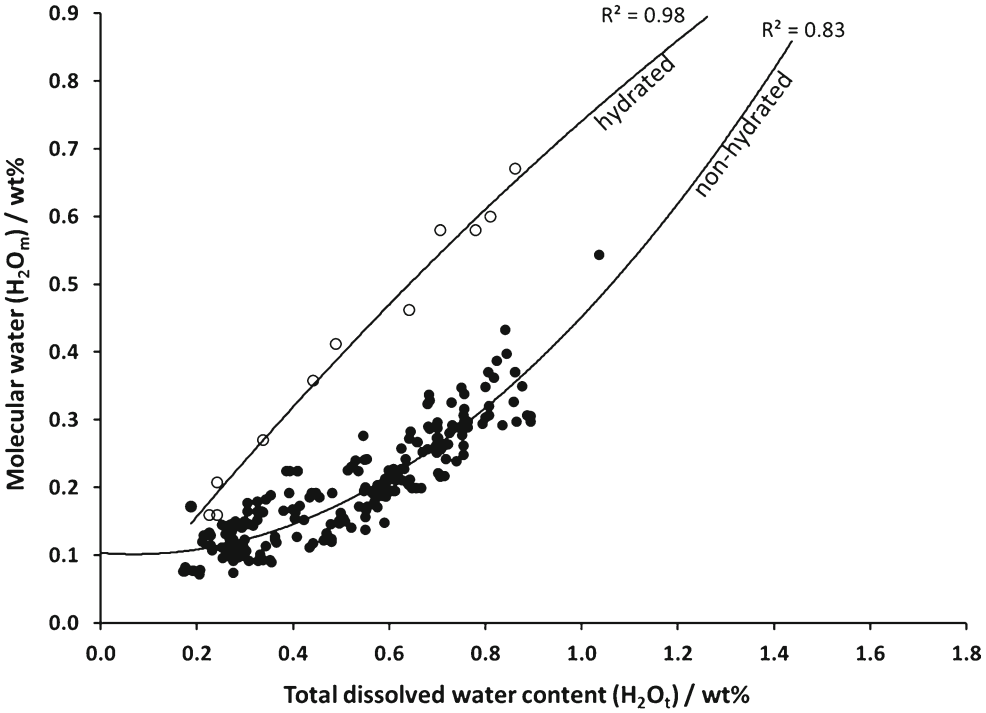

Fig. 5 A speciation graph showing FTIR data for all 40 samples. The *open circles* depict two samples considered to be hydrated, whilst the *filled in circles* represent 38 samples considered to be non-hydrated. The *lines* depict polynomial trendlines for which the R^2 values are shown

800°C for Holocene Torfajökull rhyolites of similar composition to Bláhnúkur (Gunnarsson et al. 1998). Temperature affects the SPC gradients (see section "The effect of temperature"), therefore, a range of SPCs representing different temperatures were constructed; the 800°C curve best fitted our H_2O_t data.

Discussion

Determining a palaeo-ice thickness

Figure 7a presents a range of SPCs, representing different ice thicknesses, plotted together with the measured sample water contents. At first glance, there seems to be no overall trend, but distinct trends emerge when samples are categorised by location (Fig. 7b). The Top Ridge, Feeder Dyke, Northern Slope and Grænagil follow a SPC that represents an ice surface elevation of 1,000 m (Fig. 7a), and hence 400 m ice thickness, whilst the Lobe Slope and Brandsgil follow a SPC consistent with a 1,200 m ice sheet elevation (600 m ice thickness).

A first-order interpretation to explain the spread of the FTIR data across several SPCs in Fig. 7a is that the ice thickness varied by >800 m during the eruption, and thicknesses were very different above different parts of the edifice. However, the monogenetic, small-volume eruption was probably short-lived. If we assume the eruption rate were in the range 1–5 m^3s^{-1}, based on buoyant dyke flow models and models of subglacial melting (Höskuldsson and Sparks 1997; Tuffen et al. 2007; Tuffen and Castro 2009), then the eruption timescale was probably between 0.6 and 3 years, too brief for the regional ice thickness to vary by 800 m. Formation of a significant ice cauldron during the eruption may create spatial and temporal variability in ice overburden pressure close to the eruption site, but, even in ice >500 m thick, no ice cauldron deeper than 150 m has been documented during observed Icelandic eruptions (Guðmundsson et al. 2004). Alternative interpretations to varying ice thickness must therefore be sought.

Given the reasonable fit of most data to SPCs C and D in Fig. 7a, there is the expected trend of water content decreasing upwards as the samples experience progressively lower pressures with elevation (Tuffen et al. 2010). However, this trend could also be reproduced by two alternative processes. The first is a shift from closed to open system degassing, i.e. increased volatile decoupling, which would produce decreasing vesicularity with elevation (Jaupart and Allègre 1991): This is not observed. The second is eruption from a zoned magma chamber (Jaupart 1998), which would be reflected in distinct compositional variations through the eruptive pile (McGarvie et al. 1990): Again, these are not observed (see Figs. 3 and 4). So, it is concluded that water contents decrease upwards in response to the expected progressively lower pressures with elevation (and thinner ice).

Although some groups of samples are fit well by a single SPC, there is much scatter, especially for Lobe Slope and Brandsgil samples (Fig 7). The SPC corresponding to an ice surface elevation of 1,000 m fits more of the sampling locations than any other. By comparison, the majority of the Lobe Slope and Brandsgil samples are water-rich, whereas the low-elevation A-Ridge samples are water-poor

Table 4 Estimated vesicularities and vesicle textures of the Bláhnúkur obsidians

Sample name	Mean vesicularity (%)	SD vesicularity (%)	Bubble ghosts
J1	0	–	/
B5	0	–	/
J2b	0	–	No
J2f	0	–	/
B6	18	2.3	/
B7	6	2.0	/
B8	1	2.3	/
J8	~0	2.9	/
J9	8	2.4	/
J10	7	5.8	No
B18	6	2.0	/
J6	23	0.7	/
G3a	5	2.3	/
G3end	21	1.2	/
J3	8	3.1	No
J7	8	1.9	/
J11	0	–	Yes
J13	0	–	/
J14	~0	5.0	/
B1	0	–	/
B11	0	–	/
J4	20	2.5	No
B2	17	6.9	/
B3	14	6.0	/
B4	7	5.7	/
J5	9	1.6	No
L6c	16	1.5	Yes
L7c	7	2.8	/
L8d	12	3.5	Yes
L8bott	5	1.3	Yes
L9w	17	2.4	/
L9y	10	1.5	/
L9z	19	3.2	/
L11c	6	1.3	/
B12	12	1.9	/
B13	16	3.0	/
B14	7	2.9	/
B15	8	2.5	/
B16a	14	2.6	/

0 refers to samples that were judged to be non-vesicular by eye

~0 refers to samples that were found to be 0 % vesicular to the nearest whole number using the bead technique but where a tiny percent of bubbles could be seen with the naked eye. (It is important to distinguish between samples that are near 0 % and actually 0 % vesicular for the purposes of judging whether volatile saturation has been reached)

En dash no data due to lack of measurements

Solidus no data due to lack of thin section

(Fig. 7a). As these water-rich and water-poor samples are strongly clustered by location, this hints at underlying systematic processes.

The fidelity of the results: assessing the five criteria needed to reconstruct ice thicknesses

According to Tuffen et al. (2010), five criteria need to be met in order to reconstruct ice thicknesses using the magma degassing technique. These are (1) that the magma was volatile saturated, (2) that degassing was in equilibrium, (3) that there has been no post-quenching movement of the glassy material sampled, (4) that the sample volatile concentrations are spatially homogenous and (5) that there has been no post-quenching hydration.

Volatile saturated magma

Volatile saturation is essential for the degree of magmatic degassing to faithfully indicate quenching pressures; the use of samples that quenched without having reached volatile saturation would result in an underestimate of the palaeo-ice thickness (Höskuldsson et al. 2006; Tuffen et al. 2010). Vesicular textures serve to indicate that volatile saturation has been reached; these include now-collapsed vesicles (bubble ghosts).

The lack of vesicles or bubble ghosts within the lower A-Ridge samples (Table 4) therefore suggests that volatile saturation was not achieved at this part of Bláhnúkur. This, coupled with a low dissolved water content (Table 3, Fig. 7a) suggests that either the initial water content of A-Ridge was very low (perhaps originating from a water-poor region of the magma chamber?) or that the volatiles were lost en route (open system degassing), perhaps by migration through the conduit walls at depth (Jaupart 1998). Preliminary SIMS analysis of feldspar-hosted melt inclusions within these rocks supports both of these two theories (Owen, unpublished data 2011).

The most vesicular samples are from the Lobe Slope, which are also H_2O-rich and have abundant bubble ghosts. This suggests that the lobe slope samples had relatively high initial water content and support the idea of a heterogeneous distribution of volatiles within the magma chamber.

Equilibrium degassing

In order for dissolved volatile concentrations to indicate quenching pressures equilibrium degassing needs to have occurred. The degassing model of Proussevitch and Sahagian (1996) indicates that rhyolitic magma will degas in equilibrium at ascent velocities $<1\ m s^{-1}$. The estimated volume flux of magma at Bláhnúkur is low, $<5\ m^3\ s^{-1}$ (Tuffen et al. 2008), calculated using the magma buoyancy model of Höskuldsson and Sparks (1997). This volume flux translates to a buoyant

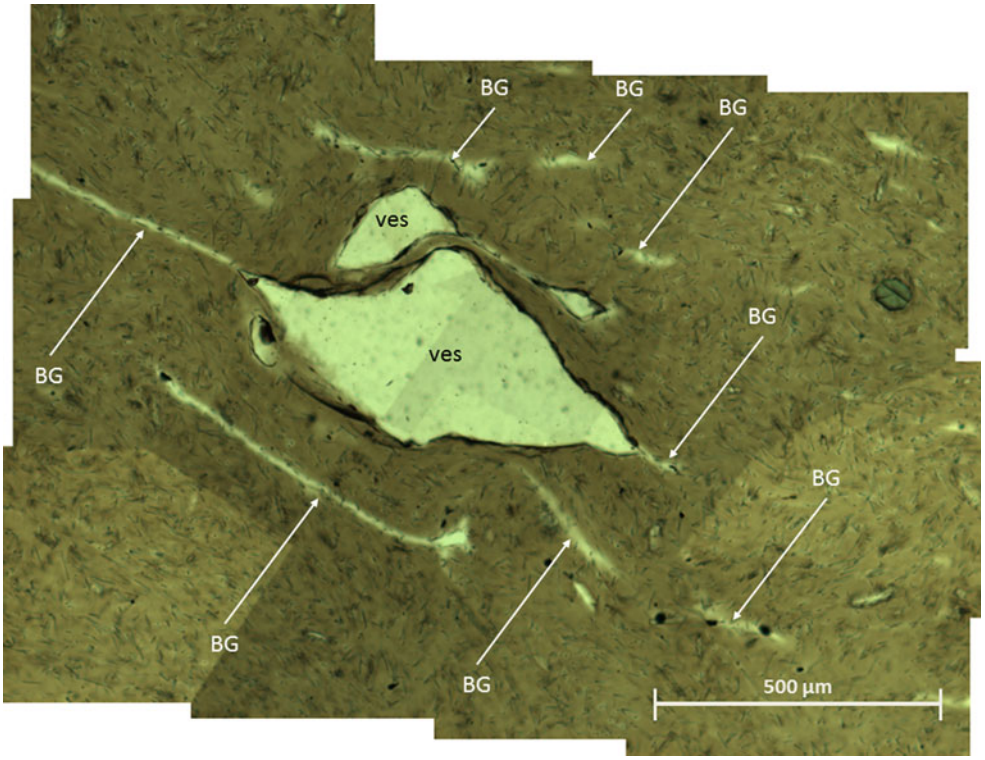

Fig. 6 A photomicrograph mosaic from sample L8d (Lobe Slope) taken in plane-polarised light. Vesicles are labelled '*ves*'; and *arrows* indicate prominent bubble ghosts, labelled '*BG*'. Pale wispy lines extend from either side of the large vesicle in the centre of the image; these indicate parts of the vesicle that have collapsed. Elsewhere in the image, similar features indicate entirely collapsed vesicles (bubble ghosts)

magma ascent velocity of <0.001 ms^{-1} assuming a dyke length and width of 1.5 km and 5 m, respectively. As this value is substantially lower than the critical ascent velocity of Proussevitch and Sahagian (1996), Bláhnúkur meets the requirements for equilibrium degassing of magmatic water.

No post-quenching movement

Samples that have changed altitude after quenching may deviate from elevation–water content trends as the pressure at which they quench will differ from the pressure indicated by their current elevations. However, care was taken to avoid collecting from locations where this may be the case. For example, the sampled lava lobes showed no obvious signs of either downslope flow or gravitational collapse (such as Breccias C and D in Tuffen et al. 2001) as their zonation displayed the overall structure of an idealised lava lobe as depicted in Fig. 6b of Tuffen et al. (2001).

Post-quenching downslope movement could, however, be an explanation for water-poor samples. Therefore, calculations were made to see how much movement would be needed to explain the water contents seen in A-Ridge. A-Ridge samples show an unexpected positive trend between altitude and water content (Fig. 7a). To restore these samples to a solubility pressure curve would create an unrealistic pattern of downslope movement distances, with the samples currently at the lowest elevation requiring the highest quenching locations and vice versa (Fig. 7a). This coupled with the lack of field evidence for downslope movement suggests that post-quenching movement cannot explain the low water contents on A-Ridge.

Magma may rise after quenching, and this could explain anomalously water-rich samples. Hydromagmatic activity may involve quenching tens to hundreds of meters below the surface (Mastin et al. 2004; Tuffen et al. 2010). However, this would trigger phreatomagmatic fragmentation, creating fragmental deposits rather than the intact lava lobes that form the bulk of the samples analysed in this study. Endogenous growth and uplift is another possible mechanism but would require 100–150 m of vertical movement, post-quenching, which is unrealistic. We are therefore satisfied that insignificant post-quenching movement has occurred.

Homogenous samples

To test the homogeneity of water within our samples, ≥5 FTIR measurements were taken per sample, with individual

Fig. 7 **a** Water content plotted as a function of elevation. *Symbol shapes* and *colours* indicate different sampling locations shown on Fig. 7b. SPCs indicate expected water contents at each elevation, for magma at 800°C with 0 ppm CO_2. SPCs *A–F* represent ice with a surface elevation of 700, 800, 1,000, 1,200, 1,400 and 1,500 masl, respectively. The *numbers* in *parenthesis* indicate ice thicknesses. The *dashed line* marks the base of Bláhnúkur. *Y* error *bars* indicate ±10 m, *x* error *bars* represent ±10 % **b** Aerial photograph of Bláhnúkur with same location colour coding as (**a**). The *black cross* indicates the mafic inclusion and *pink hexagon* the W ridge sample. *Dashed lines* indicate the four eruptive fissures proposed by Tuffen et al. (2001) and summit elevation is indicated. Aerial photograph: ©National Land Survey of Iceland

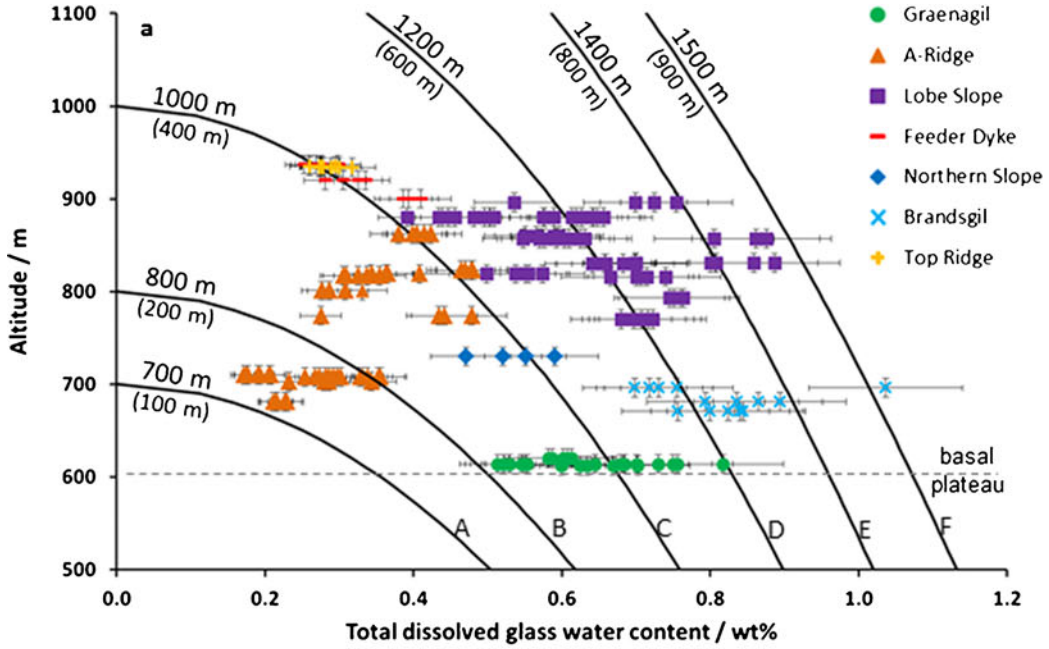
a
1100
1000
900
800
700
600
500
Altitude / m
0.0
0.2
0.4
0.6
0.8
1.0
1.2
Total dissolved glass water content / wt%
1000 m
(400 m)
1200 m
(600 m)
1400 m
(800 m)
1500 m
(900 m)
800 m
(200 m)
700 m
(100 m)
basal
plateau
A
B
C
D
E
F
Graenagil
A-Ridge
Lobe Slope
Feeder Dyke
Northern Slope
Brandsgil
Top Ridge

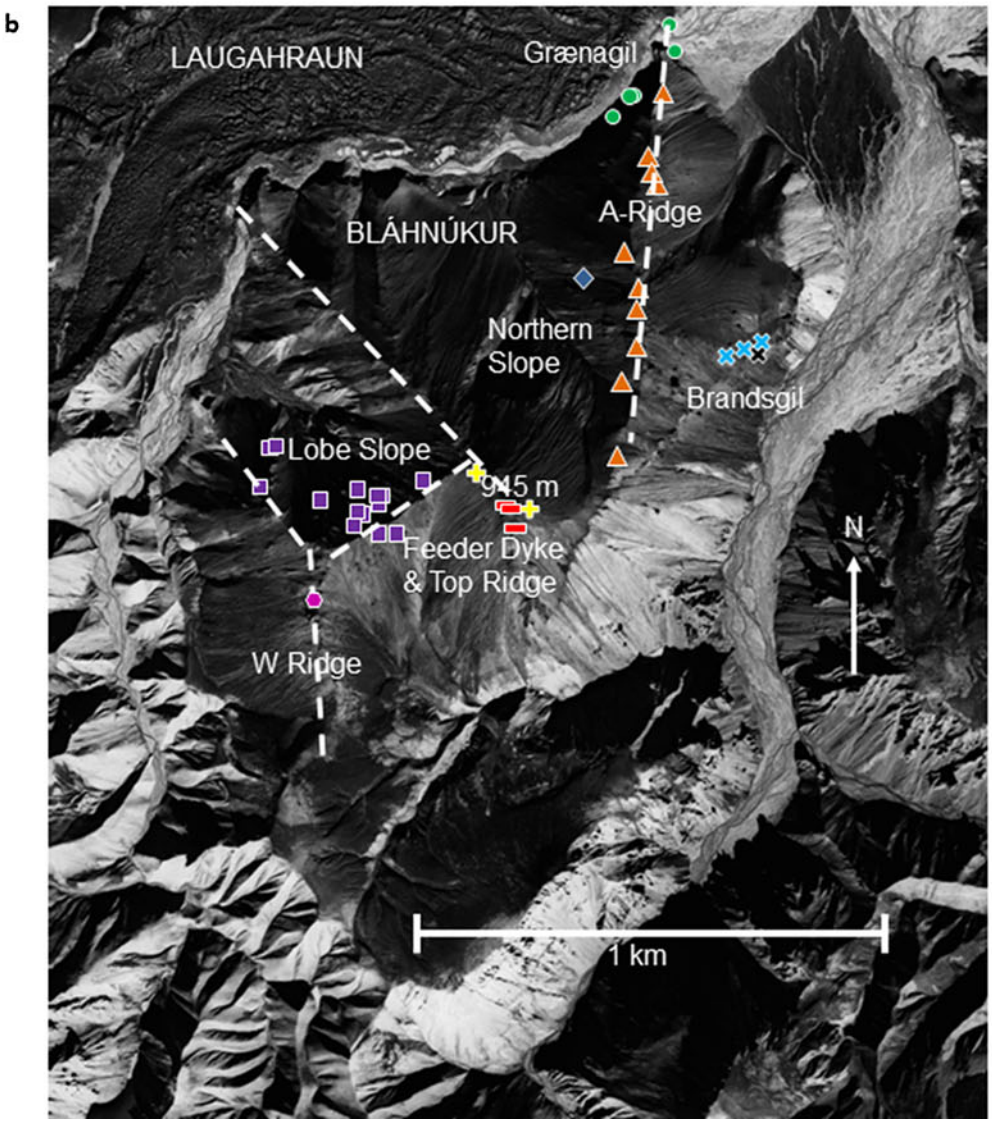
b
LAUGAHRAUN
Grænagil
BLÁHNÚKUR
A-Ridge
Northern
Slope
Brandsgil
Lobe Slope
945 m
Feeder Dyke
& Top Ridge
W Ridge
N
1 km

analyses shown as clusters of data points at uniform elevations in Fig. 7a. The tightness of clusters show that sample water contents are largely homogenous. Spatial mapping around vesicles, bubble ghosts, phenocrysts and flow bands was conducted, but no significant spatial variations were observed. Post-quenching hydration can result in highly variable H_2O_t (Fig. 5) on a sub-millimetre scale, associated with perlitic fractures (Tuffen et al. 2010). However, hydrated samples have been eliminated (see Fig. 5 and section "No post-quenching hydration"). Therefore, any variation in measured H_2O_t within considered samples probably reflects analytical errors, especially those related to slightly variable sample thicknesses (see section "The sensitivity of sample thickness").

No post-quenching hydration

When reconstructing palaeo-ice thicknesses, care must be taken not to include hydrated or perlitised samples as the post-quenching addition of meteoric water will distort reconstructions in favour of thicker ice (Tuffen et al. 2010). Only three samples showed evidence of perlitic textures in hand specimen (Table 1). However, care was chosen to select the most pristine part of these samples for producing the FTIR wafer, and indeed no perlitic textures were seen in the wafers; this is true of all samples analysed.

The speciation data (Fig. 5) indicate that most samples are non-hydrated, but hydration is suspected in two samples with anomalously high H_2O_m/H_2O_t ratios. These samples were removed from the database used for ice reconstruction modelling. The remaining 38 samples have been used to model the ice thickness, although there is some doubt about whether all A-Ridge samples meet the criteria for volatile saturation (see section "Volatile saturated magma").

Estimating quenching pressure

Which absorption coefficient to use?

The choice of absorption coefficients (ε) have a large influence on calculated H_2O and CO_2 contents. For example, for H_2O_t, using an ε of 67 $lmol^{-1}$ cm^{-1} (Stolper 1982b) compared with 100 $lmol^{-1}$ cm^{-1} (Newman et al. 1986) increases the highest water measurement from our samples by almost 50 % from 0.83 to 1.24 wt.%. This equates to a difference in ice thickness of ~800 m according to saturation pressures given by VolatileCalc (Newman and Lowenstern 2002).

There are many published rhyolitic absorption coefficients, particularly for the 3,550 cm^{-1} peak (Stolper 1982b; Newman et al. 1986; Dobson et al. 1989; Ihinger et al. 1994; Okumura et al. 2003; Leschik et al. 2004; Aubaud et al. 2009; Seaman et al. 2009). We chose to use Leschik et al. (2004)'s value of 80 $lmol^{-1}$ cm^{-1} because their samples were compositionally similar to Bláhnúkur rhyolite, both in terms of geochemistry and dissolved water content and because we consider their experimental methodology to be particularly robust.

The effect of density

The effect of glass density on calculated water contents is strong. If we use the common literature density of 2.3 gcm^{-3} for rhyolite or the density of 2.5 gcm^{-3} used for Bláhnúkur in Tuffen et al. (2001), the water content range is 0.18–1.11 wt.% and 0.17–1.03 wt.%, respectively. These differences translate to a difference of ~150 m in ice thickness, when confining pressures and equivalent ice thicknesses are calculated. We therefore measured sample density using the Archimedes method on dense samples devoid of visible vesicles and found 2.47 gcm^{-3} to be the most appropriate value.

The sensitivity of sample thickness

Although the displacement gauge used for measuring sample thickness was accurate to ±3 μm, an assumption is made that this represents the thickness of the wafer where FTIR has been carried out. Although great care was taken to try measure the H_2O and CO_2 content at the same point as the thickness measurement and to make the samples of uniform thickness, there will inevitably be some variation. Figure 8 shows the effect of thickness uncertainties of ±20 μm on the apparent H_2O content for various wafer thicknesses and various water contents.

The effect of ±20 μm uncertainty is greatest for thin samples with a high water content (and therefore peak height) and is especially strong when wafers are <100 μm thick (Fig. 8). Only four of our samples were <100 μm thick (Table 3), but two of these thin wafers were samples from Brandsgil, which appear to be anomalously water-rich. If these two samples were analysed at a point which was just 30 μm thicker than the measured value, then the resultant water contents would plot on the same solubility pressure curve as the Grænagil, Northern Slope, Top Ridge and Feeder Dyke samples (i.e. curve C in Fig. 7a). However, thickness errors of c. 80–100 μm would be needed to explain the Lobe Slope values, and it is highly unlikely we have under-estimated all of the Lobe Slope and Brandsgil samples and over-estimated the A-Ridge samples. Furthermore, we predict that because efforts were made to conduct the FTIR analysis on the same spot as the thickness measurements, errors of ±5 μm are realistic for our samples. As Figure 8 shows, the variation in calculated water contents with thickness uncertainties of ±5 μm are relatively small, especially for wafers>100 μm thick (the majority of our samples) and for water contents<1 wt.% (all of our

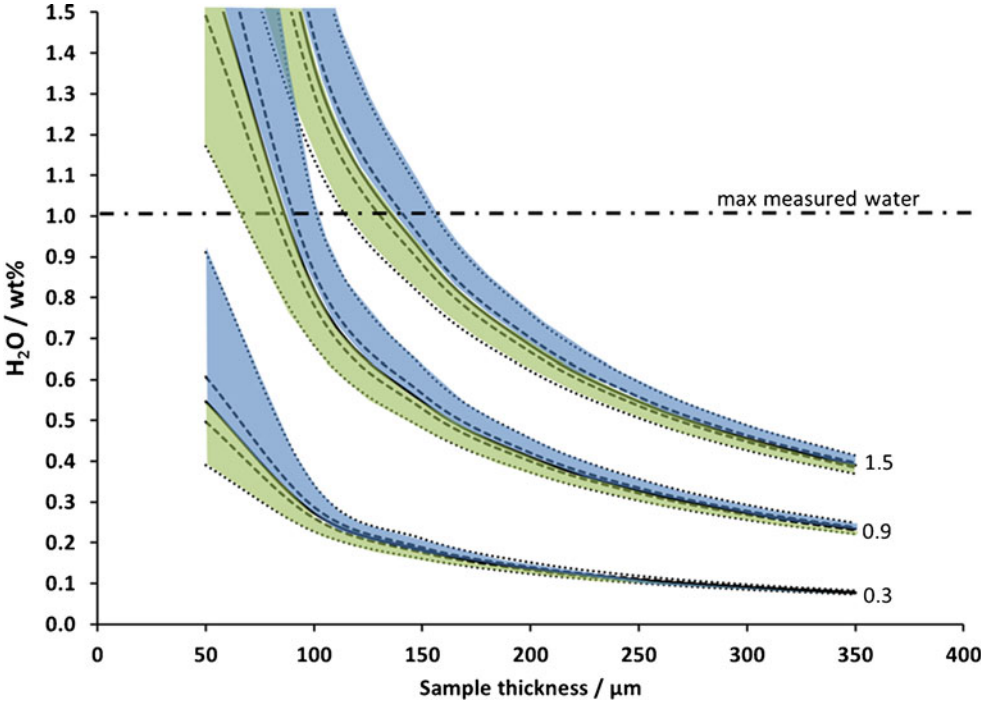

Fig. 8 Water contents plotted for sample thicknesses between 50 and 350 μm (i.e. the full range of wafers in this study), for 3,550 cm^{-1} peak heights of 0.3, 0.9 and 1.5, as labelled (i.e. the full range of absorbance levels from this study) with +/−20 μm thickness error margins, assuming a density of 2.47 gcm^{-3} and an absorption coefficient of 80 $1mol^{-1}$ cm^{-1}. The *black lines* represent the actual water content for a given sample thickness and peak height; the *dashed lines either side* represent ±5 μm and the *dotted lines* represent ±20 μm. *Blue* and *green* areas represent calculated water contents from under- or over-estimating the sample thickness by 20 μm, respectively. The *dash-dot line* indicates the maximum water content measured in our samples

samples). For these reasons, it is unlikely that variations in wafer thickness could explain the trends we see between different sampling locations (Fig. 7a), though it is probable that they could explain some of the scatter within the data.

Figure 8 illustrates that thin samples generally lead to larger uncertainties in H_2O (and CO_2) content. However, absorption peak saturation and noise are more problematic when samples are thick. The ideal sample thickness is therefore a compromise between the two and will depend on the water content of the sample.

Which solubility model to use?

Three solubility-pressure models are most frequently used due to their ease of use and wide range of parameter choices: VolatileCalc (Newman and Lowenstern (2002), H2OSOLvX1 (Moore et al. (1998) and the silicate melts H_2O–CO_2 mixed fluid solubility calculator of Papale et al. (2006). The Papale and Moore models are more compositionally sensitive than VolatileCalc, and values obtained using VolatileCalc are only approximate for water contents <1 wt.% (Tuffen et al. 2010). However, a recent review of solubility models by Moore (2008) stated that the modelling assumptions of VolatileCalc in low-pressure environments (P<100 MPa) are valid and provided that the material to which one is calculating solubilities is within the same compositional range, then VolatileCalc does an "excellent job". The major advantage of VolatileCalc is that it allows the user to input a value for CO_2 (including 0 ppm), whereas Moore's model does not allow the input of any CO_2 and Papale's model does not function well with 0 ppm. This ability to consider CO_2 is important as will be demonstrated in the section "The effect of CO_2." For this reason calculations were conducted using VolatileCalc.

The effect of CO_2

The concentration of CO_2 in a melt has a large influence on the water solubility-pressure relationships and therefore the amount of water retained in the glass (Dixon et al. 2002; Gonnermann and Manga 2005; Stevenson et al. 2009; Tuffen et al. 2010). In none of the FTIR spectra was there a resolvable CO_2 peak, therefore, the amount of CO_2 present must be below the detection limit of 30 ppm. However, 30 ppm of CO_2 can still have a large effect on water solubility, as can be seen in Fig. 9.

CO_2 is the volatile with the lowest solubility and is therefore the first to exsolve (Bailey and Hampton 1990). Its solubility is one order of magnitude lower than water (Behrens et al. 2004), therefore, if water has begun to degas (as evidenced by decreasing H_2O concentrations with elevation), then the CO_2 content should be 0 or near 0 ppm (Dixon et al. 2002). In general, volcanoes that degas at pressures <5 MPa will have virtually no CO_2 left in the magma (Tuffen et al. 2010). Since 5 MPa is equivalent to 556 m of ice, the vast majority of our samples should have degassed to this level (Fig. 7a).

Trace concentrations of CO_2 could explain some of the anomalies in water contents seen in Fig. 7a as they strongly affect SPC positions (Fig. 10). However, it is highly unlikely that magmatic CO_2 contents vary significantly (or exceed

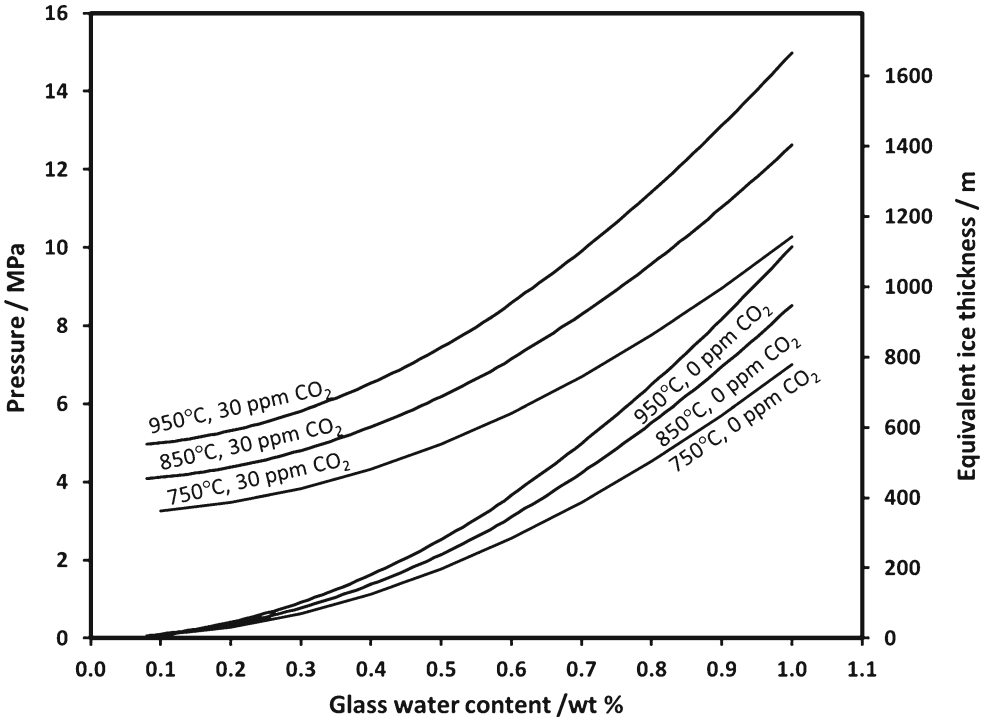

Fig. 9 The effect of temperature and CO_2 on water solubility based on calculations using VolatileCalc, modified from Tuffen et al. (2010)

a few ppm at most) as many data fit on a single SPC and even slight variations in CO_2 content would create considerable scatter in water concentration–elevation relationships.

The effect of temperature

Water solubility in magma is also temperature-dependent (Newman and Lowenstern 2002; Tuffen et al. 2010). The Bláhnúkur magma temperature is unknown but Gunnarsson et al. (1998) found a temperature of 750–800°C for Torfajokull rhyolite, and plausible eruptive temperatures for rhyolite span 750–950°C (Sparks et al. 1977). The effect of temperature is to affect the gradient of the solubility pressure curve (Fig. 9). Therefore, we constructed a range of solubility pressure curves representing different temperatures and found the 800°C curve best fits the data, a temperature consistent with the Gunnarsson et al. (1998) estimate.

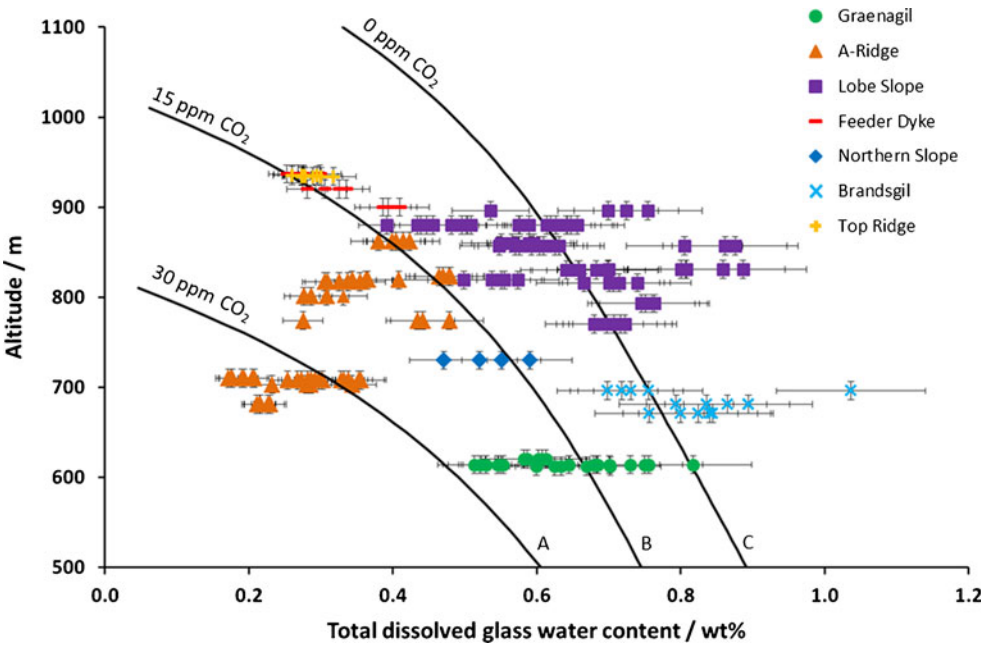

Fig. 10 A reproduction of Fig. 7a, but here all SPCs represent an ice surface at 1,200 m and T=800°C; SPCs A, B and C show the effect of 30, 15 and 0 ppm CO_2, respectively (i.e. below FTIR detection limit of ~30 ppm)

For simplicity's sake, we assume that all of Bláhnúkur erupted at 800°C. However, if parts of Bláhnúkur were erupted at >800°C, then less water would have been retained in the glass at a given pressure, which would yield lower calculated ice thicknesses. Equally, if parts erupted <800°C, then this will create water-rich samples and higher calculated ice thicknesses. Thus, the anomalies seen in Fig. 7a could be explained by the Lobe Slope and Brandsgil being erupted from particularly low temperature lavas and A-Ridge from particularly hot lavas.

Mixing of a mafic end-member could create elevated temperatures, but Bláhnúkur contains only ~1–8 % "mafic" inclusions (McGarvie 1985). Furthermore, we analysed the geochemistry of one "mafic" inclusion, and XRF data revealed it to have a SiO_2 content of 62 wt.%. Therefore any mixing of rhyolite with this intermediate composition would have produced only a very small rise in the temperature of the erupted rhyolite. Also, the Brandsgil lavas are inclusion-rich but also water-rich, which is the opposite relationship we would expect. Thus, a temperature variation due to a heterogeneous distribution of "mafic" inclusions cannot alone explain the anomalous water values seen at Bláhnúkur.

Interpreting quenching pressure

Loading by different materials

So far, we have assumed that loading was solely by ice with a uniform density of 917 kg m^{-3}. However, it is unlikely that the density of ice was a uniform 917 kg m^{-3}. It is likely that some of the ice melted to form water (Guðmundsson et al. 2004). Plus, the top ~40–100 m of a glacier tends to be permeable due to crevassing of less dense snow and firn (Cuffey and Paterson 2010).

Contrary to the Tuffen et al. (2001) model, some lava lobes may not have quenched through direct contact with the ice/meltwater at glaciostatic pressures, but instead quenched within hyaloclastite (Stevenson et al. 2011). This would lead to higher quenching pressures as hyaloclastite density exceeds that of ice, as inferred in studies by Tuffen and Castro (2009) and Stevenson et al. (2009).

Lava contains varying distributions of vesicles, and the density of the hyaloclastite will also depend on the way in which it is packed. Nevertheless, basaltic hyaloclastite is often described as having a density of 1,900 kg m^{-3} (Tuffen and Castro 2009). There is no 'standard' density for rhyolitic hyaloclastite but, using the ratio between Icelandic basalt and rhyolite densities (Höskuldsson and Sparks 1997), a hyaloclastite density of ~1,620 kg m^{-3} would be expected if vesicularity and granulometry were similar. Using this density, the water-richness of the lobes on Brandsgil can be explained by intrusive formation under 280 m of hyaloclastite, with an ice surface still at 1,000 m. To explain the degree of water-richness seen in the Lobe Slope, samples would require there to be a hyaloclastite deposit up to 1,050 masl This is 50 m higher than the ice surface and would mean that the entire loading was due to hyaloclastite and that the eruption became emergent with the overlying material having since been eroded away.

Intrusive formation is favoured by the observation that, in general, lobes occurring on ridges are more degassed than lobes occurring on slopes (that will have been more prone to erosion). In support of this, it is worth emphasising that, of the Lobe Slope samples, those on the ridges are less water-rich than those on the slope itself (Fig. 11).

The Lobe Slope is the only slope where abundant lava lobes are exposed (Fig. 2). It is highly eroded, leading to good exposure of the underlying rhyolite (Fig. 2). Lava lobes may be equally abundant on other, less eroded slopes but are currently hyaloclastite-covered. It seems plausible that the Lobe Slope lobes formed intrusively. However, the thickness of hyaloclastite required seems unrealistic as this would require the top of the Lobe Slope to have pierced an ice surface at 1,000 m elevation, and there is no field evidence supporting subaerial lithofacies or a suberial lava cap (Tuffen et al. 2001; McGarvie 2009). Furthermore, emergence should lead to near-atmospheric pressure conditions at the vent and degassing of water to ~0.1 wt.% (Tuffen and Castro 2009). Even the highest Blahnukur glasses are significantly more water-rich than this.

The water-rich samples of Brandsgil suggest the the lava body here (Fig. 7b) is a sill that intruded into hyaloclastite rather than a lava flow onto which hyaloclastite was subsequently deposited. However, again, the thickness of hyaloclastite required (280 m) seems too high. It should be noted that this value is exploiting the relative difference between the samples that follow solubility pressure curves C and D in Fig. 7a. This implies 280 m of erosion from Brandsgil and at least 170 m from the Lobe Slope, but no erosion from anywhere else sampled. This also seems unrealistic and creates an unusual profile which can be seen in Fig. 12.

Cavity pressure

The ability to reconstruct palaeo-ice thicknesses from the solubility of water hinges on the assumption that the pressure experienced by the rock is equal to the pressure of the overlying ice, i.e. that cavity pressure is equal to glaciostatic pressure (Höskuldsson et al. 2006; Tuffen et al. 2010). In reality, this may not be true, and either underpressure or overpressure may develop due to local hydrology and/or the volume budget of melting vs. erupted magma (Höskuldsson and Sparks 1997; Tuffen et al. 2007).

If overpressure were to develop, then the quenching pressure would exceed glaciostatic; this is favoured by an undrained system (Guðmundsson et al. 2004), but, at

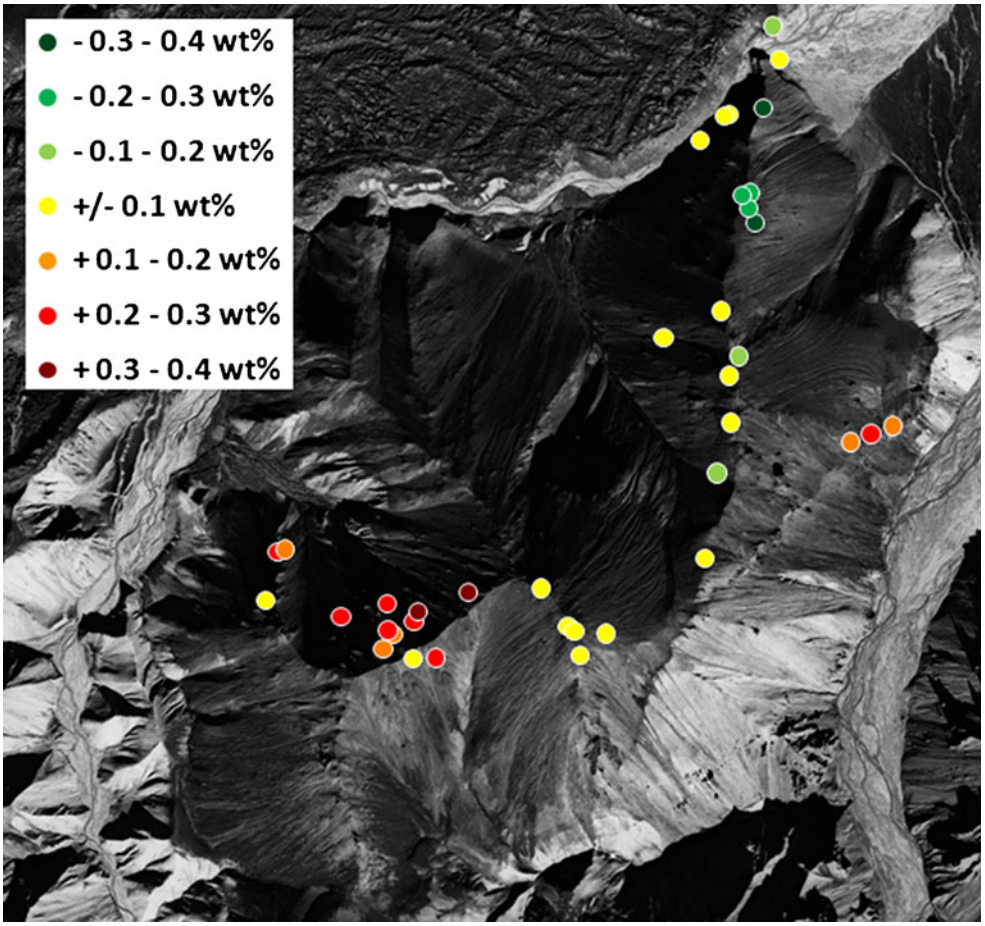

Fig. 11 Aerial map of Bláhnúkur showing the sampling locations, colour-coded according to how close the water contents are to SPC C in Fig. 7a which represents an ice surface of 1,000 m, 0 ppm CO_2 and 800°C. *Yellow symbols* indicate water contents within ±0.1 wt.% of this solubility curve, *green* samples are water-poor by comparison and *orange/red* samples are water-rich (see legend for details). Aerial photograph: ©National Land Survey of Iceland

Bláhnúkur, there is geological evidence for meltwater drainage during the eruption (Tuffen et al. 2001, 2002b). There is also no evidence to suggest why water drainage would not occur on the water-rich Lobe Slope (which is inclined at ~40°) or in Brandsgil (which is even steeper). Thus, overpressure is an unlikely explanation for the water-rich samples in Fig. 7a.

Underpressure, as described in Guðmundsson et al. (2004), Schopka et al. (2006) and Tuffen et al. (2010), is a plausible explanation for the water-poor samples seen in Fig. 7a. Efficient meltwater drainage and underpressure is a plausible scenario for A-Ridge, considering that there is a large lava body that is interpreted as a dyke and lava flow at the top of the ridge and another large coherent body, which is interpreted as a sill, directly underneath it (Fig. 7b). The formation of these structures would have provided considerable thermal energy and possibly led to a high meltwater flux sufficient to maintain open cavity conditions and low pressures (Hooke 1984).

However, this reason alone cannot be used to explain the water-poor samples of A-Ridge because if there was significant underpressure, then highly vesicular samples would have been generated, but these are absent (Table 4). This explanation only works if the A-Ridge samples also had a low pre-eruptive water content.

Reconstructing the palaeo-ice thickness at Bláhnúkur

The dissolved water contents at the bulk of the sampling locations (Top Ridge, Feeder Dyke, Northern Slope and Grænagil, plus some of the Lope Slope and high elevation A-Ridge samples) fit onto a solubility pressure curve consistent with an ice sheet surface elevation of 1,000 masl, meaning that the ice was 400 m thick at the time of the eruption (Fig. 7a). This is consistent with previous estimations of the ice thickness at Bláhnúkur, >400 m (Tuffen et al. 2001; Tuffen et al. 2007), and is only slightly less than estimates based on facies transitions at nearby tuyas (Tuffen et al. 2002a; McGarvie et al. 2006). What is more, the water contents for these samples decrease with elevation, as one would expect them to with reduced ice thickness near the top of the edifice, and the gradient of this trend is consistent with the inferred magma temperature of 800°C.

Explanations for water-poor samples

Samples from A-Ridge do not have a negative trend between water content and elevation, and the majority of samples are less water-rich than expected for a

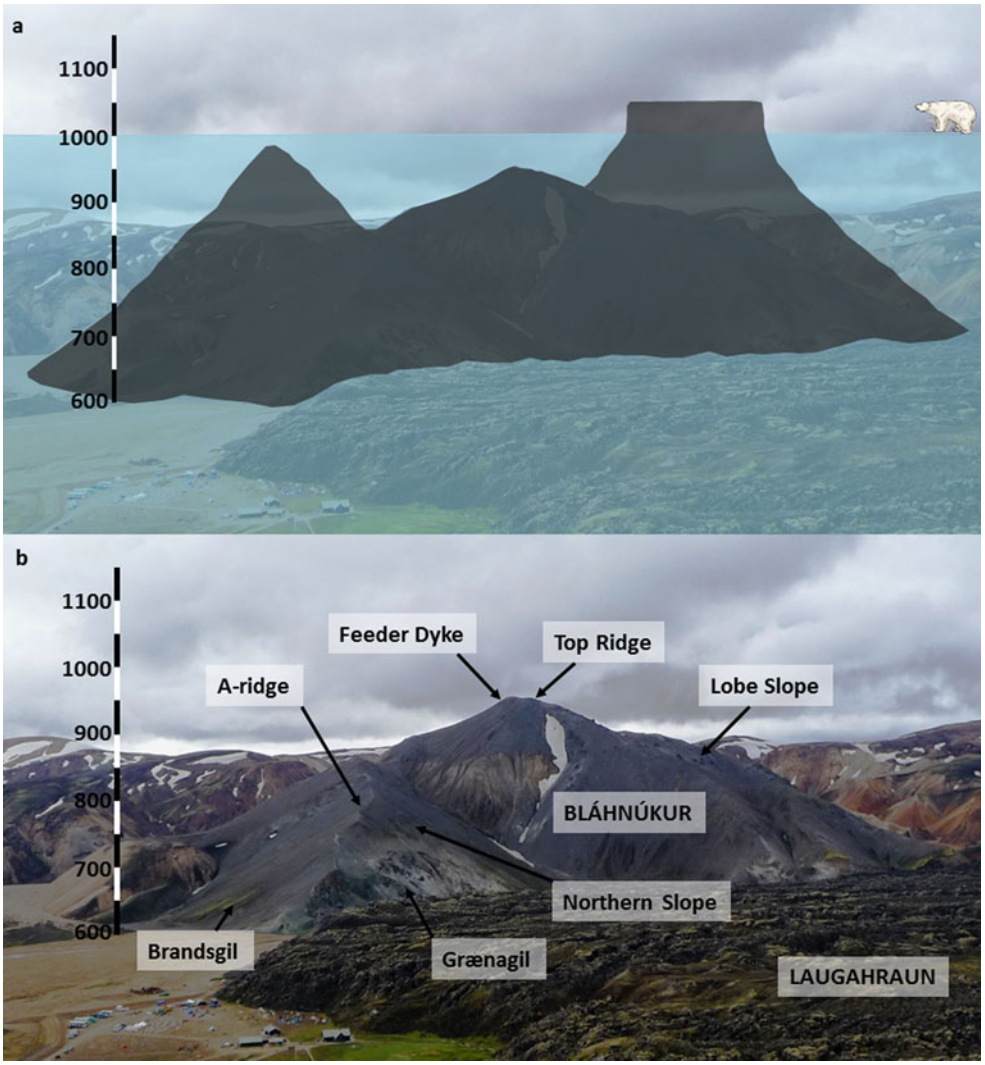

Fig. 12 **a** A hypothetical profile of what Bláhnúkur would have looked like immediately after formation with an ice surface of 1,000 m and with the additional thicknesses of hyaloclastite discussed in section "Loading by different materials." **b** what Bláhnúkur looks like today with Landmannalaugar campsite in the foreground

1,000 m ice surface elevation (Fig. 7a). One potential explanation is low pre-eruptive water content, the explanation also given (but not proven) for anomalously water-poor subglacial lavas elsewhere (Dixon et al. 2002; McGarvie et al. 2007). In contrast, Schopka et al. (2006) and Höskuldsson et al. (2006) proposed that anomalously water-poor, vesicular basaltic glasses erupted subglacially, reflected non-glaciostatic pressures (cavity underpressure), linked with subglacial meltwater drainage. Cavity underpressure was also inferred for the 1996 Gjálp eruption, based on the formation of a large ice cauldron at the southern end of the fissure (Guðmundsson et al. 2004). However, the vesicle-free nature of the lower A-Ridge samples (Table 4) means that this explanation could only be applied to Bláhnúkur, if it occurred to volatile under-saturated magma as a consequence of a low pre-eruptive water content. Therefore, we prefer the low pre-eruptive water content explanation, possibly combined with cavity underpressure.

Explanations for water-rich samples

Finding a single explanation for the water-rich samples of the Lobe Slope and Brandsgil is even more difficult. If the samples were uplifted post-quenching (endogenous edifice growth), then they must have risen 100 m if covered by lava or 150 m if covered by hyaloclastite. If the samples were erupted intrusively into hyaloclastite, then hundreds of meters of erosion are required. If the samples were erupted under thicker ice, it would have required an unrealistic 200 m vertical variation in local ice thickness. Instead, a combination of factors probably led to the elevated water contents seen on the Lobe Slope and Brandsgil. The overall trend of the water-rich samples is that of decreasing water content with elevation, which can be modelled by a single solubility pressure curve, but there is considerable variability. This suggests that there are different processes affecting the samples on different scales. We believe that loading from volcanic material was the principal factor, due to evidence of significant erosion from the water-rich

locations. With the possibility of variations in CO_2 content, temperature, ice thickness, etc., all contributing to the elevated H_2O in the Lobe Slope and Brandsgil samples; the additional hyaloclastite loading may not have been as extreme as presented in Fig. 12. These additional contributors could also account for the large degree of scatter in the Lobe Slope and Brandsgil samples, although it is likely that variation in sample thickness (Fig. 8) provides the largest degree of scatter. Furthermore, if Brandsgil quenched whilst loaded by hyaloclastite, then this suggests that the lava body there (Fig. 7b) was a sill rather than a lava flow. For this body, then, the application of H_2O and CO_2 data was able to help us identify structures that were not interpretable from field relationships.

Ice cauldrons

Ice melting and meltwater drainage during subglacial eruptions is often accompanied by the formation of a depression on the ice surface known as an ice 'cauldron' (Guðmundsson et al. 1997, 2004). The strong evidence for meltwater drainage during the eruption of Bláhnúkur (Tuffen et al. 2001) suggests that an ice cauldron likely formed over the eruptive vent. The development of an ice cauldron breaks down the assumption of a flat palaeo-ice surface and therefore the ability to reconstruct palaeo-ice thicknesses. However, the Feeder Dyke, Top Ridge, Northern Slope and Grænagil samples have solubility–pressure relationships which are consistent with a palaeo-ice surface at 1,000 m (Fig. 7a) despite these sampling locations varying from the middle to the margin of the edifice (Fig. 7b). Furthermore, the spatial distribution of discrepancy from the 1,000 m solubility pressure curve in Fig. 11 does not show lower pressure at the summit and higher pressure towards the edifice margins. Thus, if a cauldron did form during the eruption of Bláhnúkur, it must have extended over a wider area than the Bláhnúkur edifice, so that the palaeo-ice surface (or meltwater potential) appeared approximately flat for the eruption site. Since cauldron subsidence involves brittle failure and piston-like movement (Guðmundsson et al. 1997; 2004), retention of a locally flat palaeo-ice surface is a plausible scenario. An ice cauldron with a diameter >1.5 km is required to cover all of the Bláhnúkur sampling locations (Fig. 7b); an ice cauldron 3 km wide was photographed during the 1996 Gjálp eruption (Guðmundsson et al. 2004). Therefore, Bláhnúkur may have erupted under a flat ice surface that was the base of a large ice cauldron. If this were the case, then up 150 m may need to be added to the reconstructed palaeo-ice thickness, consistent with the ice cauldron depths at Gjálp (Guðmundsson et al. 2004). This would mean that the local syn-eruptive palaeo-ice surface elevation at Bláhnúkur might have been 1000 m, but original ice sheet surface elevation 1,150 m. Similar uncertainties about ice cauldron depths also affect ice thickness estimates from lithofacies transitions, and further research is needed to better constrain the factors controlling ice cauldron depths during subglacial basaltic and rhyolitic eruptions.

The appropriateness of using magma degassing to reconstruct palaeo-ice thicknesses

Table 5 lists the plausible range of parameters used to calculate quenching pressures in subglacial rhyolitic eruptions; these can lead to enormous considerable variation in the results. For example, calculated ice thicknesses above samples L9w, from the Lobe Slope, could fall anywhere between ~500 m and ~5 km. Note that, this table assumes that the water contents are purely a function of ice loading and considers none of the five criteria (e.g. hydration, or disequilibrium degassing) or various interpretations of quenching pressure (e.g. loading by volcanic material or cavity underpressure) described earlier in the discussion. Therefore, the potential range of ice thicknesses is even greater than that suggested in Table 5.

This emphasises that quantitative estimates of palaeo-ice thickness should only be made when the parameter choices can be constrained well (e.g. parameter set 1 in Table 5) and where there is good understanding of emplacement mechanisms and post-emplacement histories of lithofacies (e.g. where intrusive formation, or post-quenching collapse are possible). We believe that this has been achieved in this study of Bláhnúkur. However, it is noteworthy that the parameter values that have been selected (as discussed in section "Estimating quenching pressure") are at the lower end of the potential range (Table 5).

Table 5 also illustrates that the values obtained from dissolved H_2O, and CO_2 contents should ideally be used in conjunction with independent source data such as lithofacies mapping. For example, there are several lines of evidence that Bláhnúkur erupted entirely under ice, and yet the H_2O and CO_2 content of J1 suggests that the ice thickness was 220–240 m below the summit (using parameter sets 1 or 2 from Table 5). Equally, it is highly unlikely that there was 5 km of ice covering Bláhnúkur in the Pleistocene, as the agreed ice thickness for central Iceland during the last glacial maximum was 1,000–1,500 m (Bourgeois et al. 1998) with a plateau elevation at ~2,000 masl (Hubbard et al. 2006).

Assessment of volatile saturation pressures is useful for assessing spatial variations within eruptive deposits, and while the three sets of parameters shown in Table 5 produce very different inferred ice thicknesses, they all agree that the Lobe Slope sample suggests the greatest quenching pressure and the A-Ridge sample the smallest. All arguments put forward in the discussions section to explain the relative differences between the localities allow us to interpret how Bláhnúkur formed and how the glacier behaved at the time

Table 5 A summary of the parameters used to reconstruct the palaeo-ice thickness at Bláhnúkur and the ice thickness values obtained for three samples (J11, L9w and J1). Also shown are the parameters needed to create minimum and maximum ice thicknesses within the rhyolitic range

	Parameter set 1 (values used)	Parameter set 2 (minimum values)	Parameter set 3 (maximum values)
Absorption coefficient (l mol^{-1} cm^{-1})	80[a]	100[b]	67[c]
Density (g cm^{-3})	2.473[d]	2.5[e]	2.3[f]
Solubility model	VolatileCalc[g]	VolatileCalc[g]	Papale[h]
Temperature (°C)	800[d]	750[i]	950[i]
CO_2 (ppm)	0[j]	0[j]	30[k]
Ice elevation over J11 (thickness) (m)	1000 (400)	973 (373)	5552 (4952)
Ice elevation over L9w (thickness) (m)	1401 (801)	1154 (554)	5894 (5294)
Ice elevation over J1 (thickness) (m)	724 (124)	705 (105)	5282 (4682)

J11 is a sample from the Feeder Dyke and was the sample collected from the highest elevation—it plots on the solubility pressure curve for 400 m thick ice shown in Fig. 7a

L9w is the most water-rich sample from the Lobe Slope

J1 is the lowest elevation sample from A-Ridge which was also water-poor

[a] Leschik et al. (2004); [b] Newman et al. (1986); [c] Stolper (1982b); [d] value obtained from this study, [e] Tuffen et al. (2001); [f] Höskuldsson and Sparks (1997); [g] Newman and Lowenstern (2002); [h] Papale et al. (2006); [i] Sparks et al. 1977; [j] Dixon et al. (2002); [k] Tuffen et al. (2010)

of eruption. Thus, analysis of magma degassing processes has the potential to offer more than just a simple ice thickness estimate.

Our data highlight the need to analyse a large, widely distributed sample set, as otherwise key spatial variations in degassing will be missed. As demonstrated in Table 5, if only samples from the Feeder Dyke, the Lobe Slope or A-Ridge had been analysed, the results would have yielded three quite different palaeo-ice thicknesses.

Conclusion

In assessing the degree of magma degassing during a subglacial rhyolite eruption at Bláhnúkur, we have produced the largest data set of retained volatile contents from any subglacially erupted deposit. Glassy samples were found to contain 0.17–1.04 wt.% water, and concentrations generally decrease with elevation, consistent with the presence of an ice cap at the time of the eruption. The water contents of samples from many locations are consistent with an ice sheet 400 m thick, consistent with independent estimates. More water-rich samples may have formed intrusively, with loading by both hyaloclastite and ice. This is supported by field evidence that indicates considerable erosion of hyaloclastite from these areas. One ridge shows no systematic decrease in water content with elevation, and here, low-elevation samples are water-poor and vesicle-free, suggesting that volatile saturation was not reached and that the pre-eruptive volatile content was low in this area.

Our large data set has highlighted a number of issues concerning the use of volatile saturation models for reconstructing palaeo-ice thicknesses. Firstly, calculated pressures are highly sensitive to the chosen input parameters. Glass density and CO_2 content can be measured and magma temperature inferred but the absorption coefficient and solubility model must be chosen with care. Secondly, further variation can be introduced by both pre- and post-quenching processes (e.g. non-glaciostatic pressure, glass hydration and sample elevation changes). This highlights the importance of constraining as many parameters as possible and having a good understanding of the eruptive mechanisms of sampled facies.

Despite the complexity in our data, a simple and predictable trend of decreasing H_2O content with elevation does emerge and our estimated minimum local ice thickness of 400 m is robust, despite uncertainties about the depth of any ice cauldron that may have formed during the eruption. Our large data set has also allowed us to spot and understand anomalous values (e.g. those samples which are hydrated) and to separate those from real trends (e.g. samples erupted intrusively) that otherwise might be rejected for deviating from overall trends. This provides rich additional information about the eruptive mechanisms and environment.

Acknowledgments We would like to acknowledge the Icelandic Environment Agency, the Icelandic Centre for research and the Icelandic Institute of Natural History for fieldwork and sampling permission. JO was funded by NERC studentship NE/G523439/1, HT by NERC grants NE/G000654/1 and NE/E013740/1 and a Royal Society University Research Fellowship. DMcG acknowledges support from the Open University staff Tutor Research and Scholarship Fund. Thanks to

Ferðafélag Íslands staff at Landmannalaugar (Helga, Elín Lóa, Snæbjörn, Benedikta, Rakel, Bjarney) and Fjallafang (Nína, Smári, Orri, Sarah). Field assistance was provided by J Denton and A de Chazal and lab assistance by C Valentine, A Wilkinson, W Gosling, S Flude and N Odling. We wish to thank H Pinkerton, L Wilson, P Wynn, J Gilbert, M James, J Stevenson, P Clay and many others for their productive discussions. We are also extremely grateful to J Dixon, two anonymous reviewers and editor James White for their insightful comments.

References

Aubaud C, Bureau H, Raepsaet C, Khodja H, Withers AC, Hirschmann MM, Bell DR (2009) Calibration of the infrared molar absorption coefficients for H in olivine, clinopyroxene and rhyolitic glass by elastic recoil detection analysis. Chem Geol 262(1–2):78–86. doi:10.1016/j.chemgeo.2009.01.001

Bailey DK, Hampton CM (1990) Volatiles in alkaline magmatism. Lithos 26(1–2):157–165. doi:10.1016/0024-4937(90)90045-3

Behrens H, Tamic N, Holtz F (2004) Determination of the molar absorption coefficient for the infrared absorption band of CO_2 in rhyolitic glasses. Am Mineral 89(2–3):301–306

Blake S (1984) Magma mixing and hybridization processes at the alkalic, silicic, Torfajökull central volcano triggered by tholeiitic Veidivötn fissuring, south Iceland. J Volcanol Geotherm Res 22 (1–2):1–31. doi:10.1016/0377-0273(84)90033-7

Bourgeois O, Dauteuil O, Van Vliet-Lanoë B (1998) Pleistocene subglacial volcanism in Iceland: tectonic implications. Earth Planet Sci Lett 164(1–2):165–178. doi:10.1016/s0012-821x(98)00201-5

Cuffey K, Paterson WSB (2010) The physics of glaciers, 4th edn. Butterworth-Heinemann/Elsevier, Burlington, MA

Denton JS, Tuffen H, Gilbert JS, Odling N (2009) The hydration and alteration of perlite and rhyolite. J Geol Soc London 166:895–904. doi:10.1144/0016-76492008-007

Dixon JE (1997) Degassing of alkalic basalts. Am Mineral 82:368–378

Dixon JE, Clague DA (2001) Volatiles in basaltic glasses from Loihi Seamount, Hawaii: evidence for a relatively dry plume component. J Petrol 42(3):627–654

Dixon JE, Stolper EM (1995) An experimental study of water and carbon dioxide solubilities in mid-ocean ridge basaltic liquids. Part II: applications to degassing. J Petrol 36(6):1633–1646

Dixon JE, Filiberto JR, Moore JG, Hickson CJ (2002) Volatiles in basaltic glasses from a subglacial volcano in northern British Columbia (Canada): implications for ice sheet thickness and mantle volatiles. In: Smellie JL, Chapman MG (eds) Volcano-Ice interaction on Earth and Mars. The Geological Society, London, pp 255–271, Special Publication No. 202

Dobson PF, Epstein S, Stolper EM (1989) Hydrogen isotope fractionation between coexisting vapor and silicate glasses and melts at low pressure. Geochim Cosmochim Acta 53(10):2723–2730. doi:10.1016/0016-7037(89)90143-9

Edwards BR, Skilling IP, Cameron B, Haynes C, Lloyd A, Hungerford JHD (2009) Evolution of an englacial volcanic ridge: Pillow Ridge tindar, Mount Edziza volcanic complex, NCVP, British Columbia, Canada. J Volcanol Geotherm Res 185(4):251–275. doi:10.1016/j.jvolgeores.2008.11.015

Edwards BR, Russell J, Simpson K (2011) Volcanology and petrology of Mathews Tuya, northern British Columbia, Canada: glaciovolcanic constraints on interpretations of the 0.730 Ma Cordilleran paleoclimate. Bull Volcanol 73(5):479–496. doi:10.1007/s00445-010-0418-z

Furnes H, Fridleifsson IB, Atkins FB (1980) Subglacial volcanics—on the formation of acid hyaloclastites. J Volcanol Geotherm Res 8 (1):95–110

Gonnermann HM, Manga M (2005) Nonequilibrium magma degassing: results from modeling of the ca. 1340 A.D. eruption of Mono Craters, California. Earth Planet Sci Lett 238(1–2):1–16. doi:10.1016/j.epsl.2005.07.021

Guðmundsson MT (2005) 6. Subglacial volcanic activity in Iceland. In: Caseldine C, Russell A, Harðardóttir JÓK (eds) Developments in quaternary sciences, vol 5. Elsevier, New York, pp 127–151

Guðmundsson MT, Sigmundsson F, Bjornsson H (1997) Ice-volcano interaction of the 1996 Gjalp subglacial eruption, Vatnajokull, Iceland. Nature 389(6654):954–957

Guðmundsson MT, Sigmundsson F, Björnsson H, Högnadóttir T (2004) The 1996 eruption at Gjálp, Vatnajökull ice cap, Iceland: efficiency of heat transfer, ice deformation and subglacial water pressure. Bull Volcanol 66(1):46–65. doi:10.1007/s00445-003-0295-9

Gunnarsson B, Marsh BD, Taylor HP Jr (1998) Generation of Icelandic rhyolites: silicic lavas from the Torfajökull central volcano. J Volcanol Geotherm Res 83(1–2):1–45. doi:10.1016/s0377-0273(98)00017-1

Hooke RL (1984) On the role of mechanical energy in maintaining subglacial water conduits at atmospheric pressure. J Glaciol 30 (105):180–187

Höskuldsson A, Sparks RSJ (1997) Thermodynamics and fluid dynamics of effusive subglacial eruptions. Bull Volcanol 59(3):219–230. doi:10.1007/s004450050187

Höskuldsson A, Sparks RSJ, Carroll MR (2006) Constraints on the dynamics of subglacial basalt eruptions from geological and geochemical observations at Kverkfjöll, NE-Iceland. Bull Volcanol 68(7–8):689–701. doi:10.1007/s00445-005-0043-4

Hubbard A, Sugden D, Dugmore A, Norddahl H, Pétursson HG (2006) A modelling insight into the Icelandic last glacial maximum ice sheet. Quat Sci Rev 25(17–18):2283–2296. doi:10.1016/j.quascirev.2006.04.001

Ihinger PD, Hervig RL, Mcmillan PF (1994) Analytical methods for volatiles in glasses. Rev Mineral 30:67–121

Ihinger PD, Zhang YX, Stolper EM (1999) The speciation of dissolved water in rhyolitic melt. Geochim Cosmochim Acta 63(21):3567–3578

Jakobsson S (1997) Solubility of water and carbon dioxide in an Icelandite at 1400°C and 10 kilobars. Contrib Mineral Petrol 127(1):129–135. doi:10.1007/s004100050270

Jaupart C (1998) Gas loss from magmas through conduit walls during eruption. In: Gilbert JS, Sparks RSJ (eds) The physics of explosive volcanic eruptions. The Geological Society, London, pp 73–90, Special Publication No. 145

Jaupart C, Allègre CJ (1991) Gas content, eruption rate and instabilities of eruption regime in silicic volcanoes. Earth Planet Sci Lett 102 (3–4):413–429

Jones JG (1966) Intraglacial volcanoes of South-West Iceland and their significance in the interpretation of the form of the marine basaltic volcanoes. Nature 212(5062):586–588

Jones JG (1969) Pillow lavas as depth indicators. Am J Sci 267 (2):181–195. doi:10.2475/ajs.267.2.181

Jull M, McKenzie D (1996) The effect of deglaciation on mantle melting beneath Iceland. J Geophys Res 101(B10):21815–21828. doi:10.1029/96jb01308

Larsen G (1984) Recent volcanic history of the Veidivötn fissure swarm, southern Iceland—an approach to volcanic risk assessment. J Volcanol Geotherm Res 22(1–2):33–58. doi:10.1016/0377-0273(84)90034-9

Leschik M, Heide G, Frischat GH, Behrens H, Wiedenbeck M, Wagner N, Heide K, Geißler H, Reinholz U (2004) Determination of H_2O and D_2O contents in rhyolitic glasses. Phys Chem Glasses 45 (4):238–251

MacDonald R, McGarvie DW, Pinkerton H, Smith RL, Palavz A (1990) Petrogenetic evolution of the Torfajökull Volcanic

Complex. Iceland I Relationship between the magma types J Petrol 31(2):429–459. doi:10.1093/petrology/31.2.429
Maclennan J, Jull M, McKenzie D, Slater L, Grönvold K (2002) The link between volcanism and deglaciation in Iceland. Geochem Geophy Geosy 3(11):1062. doi:10.1029/2001gc000282
Macpherson GJ (1984) A model for predicting the volumes of vesicles in submarine basalts. J Geol 92(1):73–82
Mandeville CW, Webster JD, Rutherford MJ, Taylor BE, Timbal A, Faure K (2002) Determination of molar absorptivities for infrared absorption bands of H_2O in andesitic glasses. Am Mineral 87 (7):813–821
Mastin LG, Christiansen RL, Thornber C, Lowenstern J, Beeson M (2004) What makes hydromagmatic eruptions violent? Some insights from the Keanakāko'i Ash, Kīlauea Volcano, Hawai'i. J Volcanol Geotherm Res 137(1–3):15–31. doi:10.1016/j.jvolgeores.2004.05.015
Mathews WH (1947) Tuyas, flat-topped volcanoes in Northern British-Columbia. Am J Sci 245(9):560–570
McBirney A (1963) Factors governing the nature of submarine volcanism. Bull Volcanol 26(1):455–469. doi:10.1007/bf02597304
McGarvie DW (1984) Torfajökull: a volcano dominated by magma mixing. Geology 12(11):685–688. doi:10.1130/0091-7613(1984)12<685:tavdbm>2.0.co;2
McGarvie DW (1985) Volcanology and petrology of mixed magmas and rhyolites from the Torfajokull volcano, Iceland. PhD thesis
McGarvie DW (2009) Rhyolitic volcano-ice interactions in Iceland. J Volcanol Geotherm Res 185(4):367–389. doi:10.1016/j.jvolgeores.2008.11.019
McGarvie DW, MacDonald R, Pinkerton H, Smith RL (1990) Petrogenetic evolution of the Torfajökull Volcanic Complex. Iceland II The Role of Magma Mixing J Petrol 31(2):461–481. doi:10.1093/petrology/31.2.461
McGarvie DW, Burgess R, Tindle AG, Tuffen H, Stevenson JA (2006) Pleistocene rhyolitic volcanism at Torfajökull, Iceland: eruption ages, glaciovolcanism, and geochemical evolution. Jökull 56:57–75
McGarvie DW, Stevenson JA, Burgess R, Tuffen H, Tindle AG (2007) Volcano-ice interactions at Prestahnúkur, Iceland: rhyolite eruption during the last interglacial-glacial transition. Ann Glaciol 45 (1):38–47
Moore JG (1965) Petrology of deep sea basalt near Hawaii. Am J Sci 263(1):40–52. doi:10.2475/ajs.263.1.40
Moore JG (1970) Water content of basalt erupted on the ocean floor. Contrib Mineral Petrol 28(4):272–279. doi:10.1007/bf00388949
Moore G (2008) Interpreting H_2O and CO_2 contents in melt inclusions: constraints from solubility experiments and modeling. Rev Mineral Geochem 69(1):333–362. doi:10.2138/rmg.2008.69.9
Moore G, Vennemann T, Carmichael ISE (1998) An empirical model for the solubility of H_2O in magmas to 3 kilobars. Am Mineral 83 (1–2):36–42
Mørk MBE (1984) Magma mixing in the post-glacial veidivötn fissure eruption, southeast Iceland: a microprobe study of mineral and glass variations. Lithos 17:55–75. doi:10.1016/0024-4937(84)90006-9
Mysen BO (1977) The solubility of H_2O and CO_2 under predicted magma genesis conditions and some petrological and geophysical implications. Rev Geophys 15(3):351–361. doi:10.1029/RG015i003p00351
Newman S, Lowenstern JB (2002) VolatileCalc: a silicate melt–H_2O–CO_2 solution model written in Visual Basic for excel. Comput Geosci 28(5):597–604. doi:10.1016/s0098-3004(01)00081-4
Newman S, Stolper EM, Epstein S (1986) Measurement of water in rhyolitic glasses: calibration of an infrared spectroscopic technique. Am Mineral 71(11–12):1527–1541
Newman S, Epstein S, Stolper E (1988) Water, carbon-dioxide, and hydrogen isotopes in glasses from the Ca 1340 ad eruption of the mono craters, California—constraints on degassing phenomena and initial volatile content. J Volcanol Geotherm Res 35(1–2):75–96
Nichols ARL, Wysoczanski RJ (2007) Using micro-FTIR spectroscopy to measure volatile contents in small and unexposed inclusions hosted in olivine crystals. Chem Geol 242(3–4):371–384. doi:10.1016/j.chemgeo.2007.04.007
Ohlhorst S, Behrens H, Holtz F (2001) Compositional dependence of molar absorptivities of near-infrared OH- and H_2O bands in rhyolitic to basaltic glasses. Chem Geol 174(1–3):5–20
Okumura S, Nakashima S (2005) Molar absorptivities of OH and H_2O in rhyolitic glass at room temperature and at 400–600°C. Am Mineral 90(2–3):441–447. doi:10.2138/am.2005.1740
Okumura S, Nakamura M, Nakashima S (2003) Determination of molar absorptivity of IR fundamental OH-stretching vibration in rhyolitic glasses. Am Mineral 88(11–12):1657–1662
Papale P, Moretti R, Barbato D (2006) The compositional dependence of the saturation surface of H_2O+CO_2 fluids in silicate melts. Chem Geol 229(1–3):78–95. doi:10.1016/j.chemgeo.2006.01.013
Proussevitch AA, Sahagian DL (1996) Dynamics of coupled diffusive and decompressive bubble growth in magmatic systems. J Geophys Res 101(B8):17447–17455
Sæmundsson K (1972) Jarðfræðiglefsur um Torfajökulssvæðið. Natturufræðingurinn 42:81–99
Schopka HH, Guðmundsson MT, Tuffen H (2006) The formation of Helgafell, southwest Iceland, a monogenetic subglacial hyaloclastite ridge: sedimentology, hydrology and volcano-ice interaction. J Volcanol Geotherm Res 152(3–4):359–377. doi:10.1016/j.jvolgeores.2005.11.010
Seaman SJ, Dyar MD, Marinkovic N (2009) The effects of heterogeneity in magma water concentration on the development of flow banding and spherulites in rhyolitic lava. J Volcanol Geotherm Res 183(3–4):157–169. doi:10.1016/j.jvolgeores.2009.03.001
Sigvaldason GE, Annertz K, Nilsson M (1992) Effect of glacier loading/deloading on volcanism: postglacial volcanic production rate of the Dyngjufjöll area, central Iceland. Bull Volcanol 54(5):385–392. doi:10.1007/bf00312320
Silver L, Stolper E (1989) Water in albitic glasses. J Petrol 30(3):667–709
Silver LA, Ihinger PD, Stolper E (1990) The influence of bulk composition on the speciation of water in silicate-glasses. Contrib Mineral Petrol 104(2):142–162
Smellie JL (2000) Subglacial eruptions. In: Sigurdsson H (ed) Encyclopedia of volcanoes. Academic, San Diego, pp 403–418
Smellie JL (2008) Basaltic subglacial sheet-like sequences: evidence for two types with different implications for the inferred thickness of associated ice. Earth-Sci Rev 88(1–2):60–88. doi:10.1016/j.earscirev.2008.01.004
Smellie JL, Skilling IP (1994) Products of subglacial volcanic-eruptions under different ice thicknesses: two examples from Antarctica. Sediment Geol 91(1–4):115–129
Smellie JL, Johnson JS, McIntosh WC, Esser R, Gudmundsson MT, Harnbrey MJ, de Vries BV (2008) Six million years of glacial history recorded in volcanic lithofacies of the James Ross Island Volcanic Group, Antarctic Peninsula. Palaeogeogr Palaeoclim Palaeoecol 260(1–2):122–148. doi:10.1016/j.palaeo.2007.08.011
Sparks SRJ, Sigurdsson H, Wilson L (1977) Magma mixing: a mechanism for triggering acid explosive eruptions. Nature 267 (5609):315–318
Stevenson JA (2005) Volcano–ice interaction at Öraefajökull and Kerlingarfjöll, Iceland. PhD thesis
Stevenson JA, Smellie JL, McGarvie DW, Gilbert JS, Cameron BI (2009) Subglacial intermediate volcanism at Kerlingarfjöll, Iceland: magma–water interactions beneath thick ice. J Volcanol Geotherm Res 185(4):337–351. doi:10.1016/j.jvolgeores.2008.12.016
Stevenson JA, Gilbert JS, McGarvie DW, Smellie JL (2011) Explosive rhyolite tuya formation: classic examples from

Kerlingarfjöll, Iceland. Quat Sci Rev 30(1–2):192–209. doi:10.1016/j.quascirev.2010.10.011

Stolper E (1982a) The speciation of water in silicate melts. Geochim Cosmochim Acta 46(12):2609–2620

Stolper E (1982b) Water in silicate-glasses: an infrared spectroscopic study. Contrib Mineral Petrol 81(1):1–17

Tuffen H (2010) How will melting of ice affect volcanic hazards in the twenty-first century? Philos T R Soc A 368(1919):2535–2558. doi:10.1098/rsta.2010.0063

Tuffen H (2011) Ice–volcano interactions. In: Singh VP, Singh P, Haritash UK (eds) Encyclopedia of snow, ice and glaciers. Springer, Dordrecht, pp 625–628

Tuffen H, Castro JM (2009) The emplacement of an obsidian dyke through thin ice: Hrafntinnuhryggur, Krafla Iceland. J Volcanol Geotherm Res 185(4):352–366. doi:10.1016/j.jvolgeores.2008.10.021

Tuffen H, Gilbert J, McGarvie D (2001) Products of an effusive subglacial rhyolite eruption: Bláhnúkur, Torfajökull, Iceland. Bull Volcanol 63(2):179–190. doi:10.1007/s004450100134

Tuffen H, McGarvie DW, Gilbert JS, Pinkerton H (2002a) Physical volcanology of a subglacial-to-emergent rhyolitic tuya at Rauðufossafjöll, Torfajökull, Iceland. In: Smellie JL, Chapman MG (eds) Volcano-Ice interaction on Earth and Mars. The Geological Society, London, pp 213–236, Special Publication No. 202

Tuffen H, Pinkerton H, McGarvie DW, Gilbert JS (2002b) Melting of the glacier base during a small-volume subglacial rhyolite eruption: evidence from Bláhnúkur, Iceland. Sediment Geol 149(1–3):183–198

Tuffen H, McGarvie DW, Gilbert JS (2007) Will subglacial rhyolite eruptions be explosive or intrusive? Some insights from analytical models. Ann Glaciol 45(1):87–94. doi:10.3189/172756407782282534

Tuffen H, McGarvie DW, Pinkerton H, Gilbert JS, Brooker RA (2008) An explosive-intrusive subglacial rhyolite eruption at Dalakvísl, Torfajökull, Iceland. Bull Volcanol 70(7):841–860. doi:10.1007/s00445-007-0174-x

Tuffen H, Owen J, Denton J (2010) Magma degassing during subglacial eruptions and its use to reconstruct palaeo-ice thicknesses. Earth-Sci Rev 99(1–2):1–18. doi:10.1016/j.earscirev.2010.01.001

Westrich HR, Eichelberger JC (1994) Gas transport and bubble collapse in rhyolitic magma: an experimental approach. Bull Volcanol 56(6–7):447–458

Yokoyama T, Okumura S, Nakashima S (2008) Hydration of rhyolitic glass during weathering as characterized by IR microspectroscopy. Geochim Cosmochim Acta 72(1):117–125. doi:10.1016/j.gca.2007.10.018

Zhang Y (1999) H_2O in rhyolitic glasses and melts: measurement, speciation, solubility, and diffusion. Rev Geophys 37:493–516